

# Novel state with broken time reversal symmetry due to light-matter interaction in samarium hexaboride

*\*Partha Goswami and Udai Prakash Tyagi*

*D.B.College, University of Delhi, Kalkaji, New Delhi-110019, India*

*\*Email of the corresponding author: [physicsgoswami@gmail.com](mailto:physicsgoswami@gmail.com)*

*Email of the second author: [uptyagi@yahoo.co.in](mailto:uptyagi@yahoo.co.in)*

**Abstract** We show that the compound samarium hexaboride is a strong topological insulator using the eigenvalues of the space inversion operator. A Dirac cone like feature in the surface state energy spectra is observed in the absence of magnetic impurities. We also show that the system is in the quantum anomalous Hall phase when impurities are present. We further show that access to a novel state with broken time reversal symmetry is possible due to the normal incidence of circularly polarized optical field on the surface of the compound even when impurities are absent.

## 1. Introduction

The recipe required for the formation of the topologically non-trivial surface states in a generic topological Kondo Insulator (GTKI)[1-3], such as  $\text{SmB}_6$ , are band inversion by hybridization and strong spin-orbit coupling. The latter does not break the time reversal symmetry (TRS). The strong correlation effects and diverse surface conditions make the GTKI system extremely complicated - almost a Gordian knot. This communication is on a topical issue of the mixed valence compound  $\text{SmB}_6$ —a narrow gap topological Kondo insulator (TKI) which, with a high-temperature metallic phase, transforms into a paramagnetic charge insulator below 45 K. These are a particular class of strongly-interacting heavy-fermion materials. The origin of the itinerant electron Fermi surface (FS), originating from the in-gap states in GTKI, is still a mystery. Quite a few works related to its peculiarities are discussed in section 5. It has been suggested [1,2], as well as there is mounting evidence [4-6] during the past several years, that  $\text{SmB}_6$  is a strong topological insulator. This has generated great deal of excitement in the condensed matter physics community and it still remains a matter of intense debate [7]. The supporting evidence for the TKI scenario [4-6] notwithstanding, there is no jury-verdict regarding the nature of the bulk and surface states of  $\text{SmB}_6$  [7-9]. In this communication we show conclusively that the  $\text{SmB}_6$  surface state is topologically non-trivial. The reason being the material band structure features odd numbers of pair intersections at time reversal invariant momenta (TRIMs). The moderate disorder cannot remove such pair-surface-state crossings (SSCs) which correspond to the topological index  $Z_2 = -1$  ( $\nu_0 = 1$ ).

We consider extension of the slave boson (SB) mean-field-theoretic version of the periodic Anderson model (PAM) [3, 10,11] for a GTKI like  $\text{SmB}_6$  on a simple cubic lattice with one spin-degenerate orbital per lattice site each for  $d$  and  $f$  electrons in the long wavelength limit. Assuming the presence of the ferromagnetic magnetic impurities in our system, we introduce

exchange interaction ( $M$ ) in the model Hamiltonian. The Hamiltonian is written down in the Dirac basis similar to the Bernevig–Hughes–Zhang (BHZ) model presented over a decade and half ago for quantum wells. We observe a Dirac cone like feature at zero momentum in the surface state energy spectra obtained using this Hamiltonian for  $M = 0$ . Thereafter, we obtain the  $Z_2$  invariant using the eigenvalues of the space inversion operator in the Fu-Kane framework [12]. We obtain  $Z_2 = -1$ . This shows that the system is a strong topological insulator for  $M = 0$ . We have also calculated the Chern number to show that the system is in the quantum anomalous Hall (QAH) phase when  $M \neq 0$ . It must be mentioned here that the ground state of the compound  $\text{SmB}_6$  (a prominent TKI) has been shown to be a quartet state [13]. As we shall see below, despite this, our low-energy model would be sufficient to capture important features of  $\text{SmB}_6$ .

The polarized periodic optical field provides a potent modus operandi to carry out theoretical proposition and experimental realization, manipulation, and detection of diverse unconventional/novel optical and electronic properties of materials, such as the realization of novel quantum phases without static counterparts like light induced quantum anomalous phase (QAH) phase [14], the topological phase transitions in semi-metals [15-20], the Floquet engineering of magnetism in topological insulator thin films [21,22], and so on. The exotic Floquet topological phases with a high tunability could be realized using this highly efficient and promising platform by band-structure engineering. In fact, there has been an upsurge on experimental front in the search for topological states, in solid state [23], cold-atom [24] and optical systems [25], which are driven periodically. The circularly polarized optical field (CPOF) is described by a time-periodic (time period =  $T = 2\pi/\omega$  where  $\omega$  is the frequency of light) gauge field. Upon using the Peierls substitution, lattice electrons couple to the electromagnetic gauge field. In the presence of COPF, the thin film Hamiltonian  $H_{\text{surface}}$ , apart from breaking the time reversal invariance (TRS), becomes periodic in time. One can now transform the time-dependent Hamiltonian problem to a time-independent one using the Floquet's theorem [26-29]. Analogous to the Bloch theory, a solution for the time-dependent Schrodinger equation of the system is obtained here involving the Floquet quasi-energy and the time-periodic Floquet state with the periodicity  $T$ . The Floquet state could be expanded in a Fourier series which makes us arrive at an infinite dimensional eigenvalue equation in the Sambe space [26]. The circularly polarized light incident upon the film may be described by a time-varying gauge field  $\mathbf{A}(t)$ . Once we have included a gauge field, it is necessary that we make the Peierls substitution  $H_{\text{surface}}(t) = H_{\text{surface}}\left(\mathbf{k} - \frac{e}{\hbar}\mathbf{A}(t)\right)$ . In view of the Floquet theory [26-29], in the high-frequency limit, a thin film system, irradiated by the circularly polarized radiation, can be described by an effective, static Hamiltonian. We make use of the Floquet theory in section 4, in the high-frequency limit, to investigate the thin film system. Interestingly, the optical field leads to the emergence of a phase where the time reversal symmetry (TRS) is broken even when  $M = 0$ . The conclusive evidence of this phase being quantum spin Hall (QSH) phase will be presented in future by calculating the spin Chern number [30]. In the reference [30], a detailed exposition of the TRS-broken quantum spin Hall effect could be found.

Our minimalistic bulk Hamiltonian captures essential physics of GTKI in the presence of the coulomb repulsion  $U_f$  ( $\gg t_{d1}$ ) between  $f$  electrons on **the** same site, and the spin-orbit hybridization  $V$ . The terms  $(t_{d1}, t_{f1})$  are the  $NN$  hopping parameter for  $d$  and  $f$  electrons. The band warping factor, usually associated with the Hamiltonian of a topological insulator, has not been considered here for the mathematical simplicity. There are three parameters  $(b, \lambda, \xi)$  of the SB theory [3]. The method to obtain them is explained clearly in ref. [3]. We never-the-less summarize briefly below to make this paper self-contained. The constraint  $U_f \gg t_{d1}$  imposes a non-holonomic constraint, viz. the exclusion of the double occupancy, which is very difficult to manipulate. The SB- framework provides a platform to reformulate this nonholonomic constraint into a holonomic constraint that can be implemented with a Lagrange multiplier. Here, an electron annihilation operator is written as the product of a spinless boson creation operator (SB) and a spinful fermion annihilation operator (We represent them by annihilation operators  $f_{k,\tau}^\dagger = (b^\dagger c_{k,\tau})$  in momentum space. Here, the index  $\tau$  ( $= \uparrow, \downarrow$ ) represents the spin.). This basically corresponds to the assumption that the annihilation of an electron is equivalent to simultaneous creation of a slave-bosonic hole and annihilation of a fermionic spinon. In the present SB framework, we make the further assumption that the slave boson field ( $b$ ) at each lattice site can be replaced by a  $c$ -number. The complications associated with the large on-site repulsion ( $U_f \gg t_{d1}$ ) between the  $f$ -electrons is conveniently circumvented in the SB theory by imposing the holonomic constraint  $\sum_\tau (c_\tau^\dagger c_\tau) = 1 - b^2$  at a site to remove the double occupancy. The term  $\lambda [\sum_{k,\tau = \uparrow, \downarrow} (c_{k,\tau}^\dagger c_{k,\tau}) + N_c (b^2 - 1)]$ , where  $N_c$  ( $N_d$ ) is the number of  $c$ -fermions ( $d$ -fermions) and  $N_c = N_d$  required for the formation of Kondo singlet states between  $d$  and  $c$  fermions at each lattice site, to be added to the system Hamiltonian to enforce the constraint on the pseudo-particles due to the infinite on-site Coulomb repulsion. Therefore, the signature of the assumption “large on-site repulsion ( $U_f \gg t_{d1}$ ) between the  $f$ -electrons” is carried over by the parameters  $\lambda$  and  $b$ . The constant term  $\lambda N_c (b^2 - 1)$  in the Hamiltonian is to be dropped here-in-after as it has no significance in the calculation below. Moreover, we neglected the dynamics of the boson field completely as the light slave boson creation and destruction operators were replaced by a  $c$ -number ‘ $b$ ’. This approximation reduced the system to a non-interacting one with the bulk spectral gap dependent on the parameters  $(b, \lambda, \xi, V)$ . Whereas the first two parameters took care of the strong correlation effect between the  $f$ -electrons, the hybridization parameter  $V$  is the harbinger of a topological dispensation. The term  $\xi$  enforces the fact that there are equal number of  $d$  and  $f$  fermions. In order to have a Kondo insulator, formation of singlet states between  $d$  and  $f$  fermions is needed at each lattice site. This means that the number of  $d$  and  $f$  fermions are equal on average. The total parameters are slave-boson field  $b$ , auxiliary chemical potentials  $\xi$  and  $\mu$  ( $\mu$  is a free parameter), and the Lagrange multiplier  $\lambda$ . One obtains equations for the parameters  $(b, \lambda, \xi)$  minimizing the thermodynamic potential per unit volume. We find that  $\lambda = -6t_{f1} + 6b^2t_{f1}$ , and  $\xi = -3t_{d1} + 3t_{f1}$ . The admissible value of  $b^2$  is  $1^-$ .

The paper is organized as follows: In section 2, we obtain the surface state band spectrum in slave-boson formalism. We show that the surface state Hamiltonian corresponds to Qi-Wu-Zhang (QWZ) model[31-33] in the absence of the magnetic impurities. As shown by these authors, the situation corresponds to QSH state. In section 3, we calculate  $Z_2$  invariant using the eigenvalues of the space inversion operator with in the Fu-Kane framework [12]. In section 4, we are able to show the emergence of a novel phase with broken-TRS by the normal incidence of tunable CPOF even when  $M = 0$ . For this purpose, we start with a low-energy two-dimensional, time-dependent Hamiltonian. We make use of the Floquet theory in the high-frequency limit to investigate the system. The TKI has a bulk gap due to hybridization between localized and conduction electrons. A mystery centers on the existence of the bulk in-gap states of the system. For example, quantum oscillations in  $\text{SmB}_6$  appear in magnetization but not in resistivity, the lack of electrical transport signature in epitaxial thin films in contrast with that in bulk, etc.. We point out these issues as a motivation for further investigation and ones related to our communication in section 5. The paper ends with very brief concluding remarks.

## 2. Surface State Band Spectrum in slave-boson formalism

We consider below extension of the slave boson (SB) mean-field-theoretic version of the periodic Anderson model (PAM) [3,10,11] for a (topological) Kondo insulator on a simple cubic lattice with one spin-degenerate orbital per lattice site each for  $d$  and  $f$  electrons. The SB protocol has been summarized below. In momentum( $\mathbf{k}$ )-space, we represent them by creation (annihilation) operators  $d_{\mathbf{k},\tau}^\dagger$  ( $d_{\mathbf{k},\tau}$ ) and  $f_{\mathbf{k},\tau}^\dagger = b c_{\mathbf{k},\tau}^\dagger$  ( $b c_{\mathbf{k},\tau}$ ), respectively. Here, the index  $\tau$  ( $= \uparrow, \downarrow$ ) represents the spin. The Hamiltonian  $H_{PAM}$  consists of three parts, namely, the hopping of the individual orbitals, the hybridization parameter  $V$  between  $d$  and  $f$  orbitals, and an onsite repulsion of  $f$  electrons ( $\mathfrak{N}_{int}$ ). The exchange energy  $M$  due to magnetic impurities will be added later. The Hamiltonian in ref.[3], with a cavalcade of ingredients on a simple cubic lattice in momentum-space, is as follows:

$$H_{PAM}(b, \lambda, \xi) = \sum_{\mathbf{k}, \tau = \uparrow, \downarrow} \widetilde{E}_k^d(\mu, \xi) d_{\mathbf{k},\tau}^\dagger d_{\mathbf{k},\tau} + \sum_{\mathbf{k}, \tau = \uparrow, \downarrow} \widetilde{E}_k^f(\mu, b, \lambda, \xi) c_{\mathbf{k},\tau}^\dagger c_{\mathbf{k},\tau} + b \sum_{\mathbf{k}, \tau = \uparrow, \downarrow} \{F_{\tau = \uparrow, \downarrow}(\mathbf{k}) \langle d_{\mathbf{k},\tau}^\dagger c_{\mathbf{k},\tau} \rangle + \text{H.C.}\} + \lambda N_c (b^2 - 1) + \mathfrak{N}_{int} \quad (1)$$

$$\widetilde{E}_k^d(\mu, \xi) = -\mu - \xi - [2t_{d1} c_1(\mathbf{k}) + 4t_{d2} c_2(\mathbf{k}) + 8t_{d3} c_3(\mathbf{k})], \quad \mathbf{k} = (k_x, k_y) \quad (2)$$

$$\widetilde{E}_k^f(\mu, b, \lambda, \xi) = -\mu + \xi - b^2 [-\epsilon_f + 2t_{f1} c_1(\mathbf{k}) + 4t_{f2} c_2(\mathbf{k}) + 8t_{f3} c_3(\mathbf{k})] + \lambda, \quad (3)$$

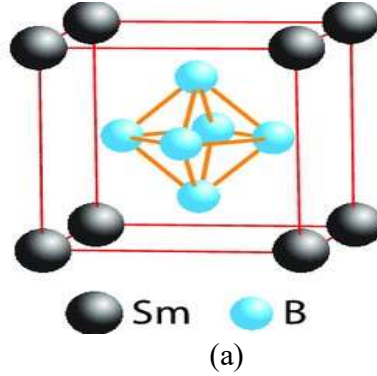
$$c_1(\mathbf{k}) = (\cos k_x a + \cos k_y a + \cos k_z a), \quad (4)$$

$$c_2(\mathbf{k}) = (\cos k_x a \cdot \cos k_y a + \cos k_y a \cdot \cos k_z a + \cos k_z a \cdot \cos k_x a), \quad (5)$$

$$c_3(k) = (\cos k_x a . \cos k_y a . \cos k_z a), \quad (6)$$

The last term in (1) is  $\mathfrak{N}_{int} = U_f \sum_{i(\text{site index})} f_{i\uparrow}^\dagger f_{i\uparrow} f_{i\downarrow}^\dagger f_{i\downarrow}$ . As one can see from (1), the dispersion of the  $f$ -electron is renormalized by  $\lambda$  and its hopping amplitude by  $b^2$ . Moreover, the hybridization amplitude is also renormalized by the  $c$ -number  $b$ . Since the  $f$ - and  $d$ -states have different parities, the momentum-dependent form-factor matrix  $F_{\tau=\uparrow,\downarrow}(k)$  involved in the third term in (1) must be odd:  $F_{\tau=\uparrow,\downarrow}(-k) = -F_{\tau=\uparrow,\downarrow}(k)$ . This is required in order to preserve time reversal symmetry (TRS), as the matrix involves coupling with the physical spin of the electron. Therefore, we write  $F_{\tau=\uparrow,\downarrow}(k) = 2V(\mathbf{s}(k) \cdot \boldsymbol{\tau}')$ , where  $V$  is a constant parameter characterizing the spin-orbit hybridization,  $\mathbf{s}(k) = (\sin k_x a, \sin k_y a, \sin k_z a)$  and  $\boldsymbol{\tau}' = (\tau_x, \tau_y, \tau_z)$  are the Pauli matrices in spin space. The terms  $(t_{d1}, t_{f1})$ ,  $(t_{d2}, t_{f2})$ , and  $(t_{d3}, t_{f3})$ , respectively, are the  $NN$ ,  $NNN$ , and  $NNNN$  hopping parameters for  $d$  and  $f$  electrons;  $\epsilon_f$  is the onsite energy of the  $f$  electrons and  $N_c$  is the number of lattice sites for these electrons.

In Figure 1(a), we have shown a diagrammatic representation of  $\text{SmB}_6$  crystal structure with cubic lattice constant  $a = 0.413$  nm. The Sm ions are located at the corners and the  $\text{B}_6$  octahedron at the center of the cubic lattice. In Figure (b) and (c), we have plotted the bulk band energies (eigenvalues of (1)) of the present TKI system in the insulating phase (where  $t_{f1}$  is negative) assuming the quasi-particles non-interacting; the spin-orbit hybridization is included in Figure 1(c). The system shows the bulk metallic as well as the bulk insulating phases determined by the sign of  $t_{f1}$ . It is positive for the former and negative for the latter phase [3]. The negative sign of  $t_{f1}$  is also necessary for the band inversion, which induces the topological state [3]. Through-



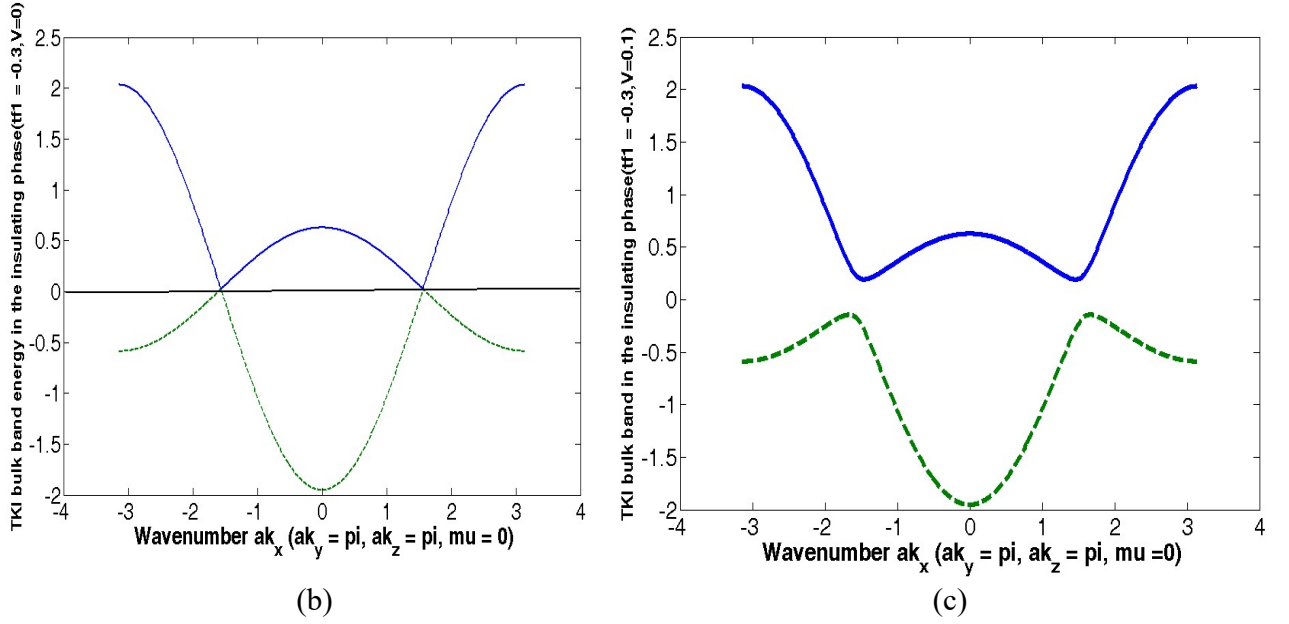


**Figure 1. (a)** A diagrammatic representation of SmB<sub>6</sub> crystal structure with cubic lattice constant  $a = 0.413$  nm. The Sm ions are located at the corners and the B6 octahedron at the center of the cubic lattice. **(b), (c)** The plots of the bulk band energies (eigenvalues of Eq. (1)) of the present TKI system in the insulating phase assuming the quasi-particles non-interacting. The hybridization parameter  $V$  is zero in (b), whereas it is 0.1 in (c). The latter one represents an insulating bulk. The numerical values of the parameters used in the plots are  $t_{d_1} = 1$ ,  $t_{f_1} = -0.3$ ,  $t_{d_2} = 0.01$ ,  $t_{f_2} = 0.01$ ,  $t_{d_3} = 0.001$ ,  $t_{f_3} = 0.001$ ,  $\epsilon_f = -0.02$ ,  $V = (0, 0.1)$ ,  $b = 0.98$ ,  $\mu = 0$ , and  $U_f \gg t_{d_1}$ .

out the paper, we choose  $t_{d_1}$  to be the unit of energy. The numerical values of the parameters used in the plots are  $t_{d_1} = 1$ ,  $t_{f_1} = -0.3$  (negative value ensures insulating bulk),  $t_{d_2} = 0.01$ ,  $t_{f_2} = 0.01$ ,  $t_{d_3} = 0.001$ ,  $t_{f_3} = 0.001$ ,  $\epsilon_f = -0.02$ ,  $V = (0, 0.1)$ ,  $b = 0.98$ ,  $\mu = 0$ , and  $U_f = 0$ . Here since the coulomb repulsion  $U_f$  between  $f$  electrons on the same site is taken into account, the correlation effect is not missing. We do find that  $V = 0$  ( $V \neq 0$ ) case does correspond to band crossing (avoided crossing) - an essential feature of SmB<sub>6</sub>. All energies in our calculation/graphical representation below are expressed in units of the first neighbor hopping  $t_{d_1}$  for d-electrons as this corresponds to the kinetic energy of these itinerant electrons and therefore the most dominant.

We shall treat the model Hamiltonian (1) in the long wave-length or low-energy limit below. In the above limit, the following replacements are necessary:

$$\sin(a_j k_j) \rightarrow a_j k_j + O(a_j^3 k_j^3), \cos(a_j k_j) \rightarrow (1 - (\frac{1}{2} a_j^2 k_j^2) + O(a_j^4 k_j^4)) \quad (7)$$

where  $j = (x, y, z)$ , and  $a_j$  is the lattice constant along  $j$  direction. Furthermore, in order to obtain surface state Hamiltonian ( $H_{\text{surface}}(k, \lambda, \mu, \xi, b)$ ) we make the replacement  $ak_z \rightarrow -ia \partial_z$  and look for states localized within the surface  $z = 0$  of the form  $\exp(-i\chi z)$ . Furthermore, we seek such a value of the unknown wave number  $\chi$  ( $\chi = -iq, q > 0$ ) for which the exponential

$\exp\left(-\frac{aqz}{a}\right) \ll 1$  for  $z > 0$ . For example, if we assume  $aq \sim 1$  the exponential  $\exp\left(-\frac{aqz}{a}\right) \sim \exp(-10)$ , i.e vanishingly small, for  $z \sim 50\text{nm}$  given that  $\text{SmB}_6$  crystal structure with cubic lattice constant  $a = 0.413 \text{ nm}$  (Figure 1(a)). Therefore,  $\chi = -iq, q > 0$  ensures a decaying term for  $z > 0$  in the surface states. For  $z < 0$ , the exponential will be  $\exp\left(\frac{aq|z|}{a}\right)$ . This implies that, in  $\text{SmB}_6$ , the surface state possesses much greater penetration depth unlike that in  $\text{Bi}_2\text{Se}_3$  (the penetration depth  $\sim 5\text{-}10 \text{ nm}$ ).

We assume the presence of the ferromagnetic magnetic impurities (FMI) in our system under consideration. We model the required interaction between an alien MI moment and the electrons in the system with coupling term  $(J \sum_m S_m \cdot s_m)$ , where  $S_m$  is the  $m$  th-site impurity spin,  $s_m = \sum_{\tau} \left(\frac{1}{2}\right) o_{m,\tau}^\dagger \tau_z o_{m,\tau}$ ,  $o_{m,\tau}$  is the electron annihilation operator at site- $m$  and spin-state  $\tau$  ( $=\uparrow, \downarrow$ ) and  $\tau_z$  is the  $z$ -component of the Pauli matrices. We make the approximation of treating the impurity spins as classical vectors. The latter is valid for  $|\mathbf{S}| > 1$ . We absorb the magnitude of the impurity spin into the ferromagnetic coupling constant  $J$  and write  $M = |J||\mathbf{S}|$ . Upon including the exchange coupling  $M$ , in the basis  $(d_{k,\uparrow}^\dagger \ bc_{k,\downarrow}^\dagger \ d_{k,\downarrow}^\dagger \ bc_{k,\uparrow}^\dagger)^\top$ , from above we find

$$h_{\text{surface}}(k, \chi, \mu, b, M) = (\epsilon(k, \chi, \mu, b)) \sigma_0 \otimes \tau_0 + A_1 a k_x \sigma_z \otimes \tau_x + A_1 a k_y \sigma_z \otimes \tau_y + \vartheta(k, b, \chi) \sigma_0 \otimes \tau_z + M \sigma_z \otimes \tau_z + \left(\frac{1}{2}\right) [-i A_1 a q (\sigma_x + i\sigma_y) \otimes \tau_x + i A_1 a q (\sigma_x - i\sigma_y) \otimes \tau_x] \quad (8)$$

$$A_1 = 2Vb, \mathbf{k} = (k_x, k_y), k^2 = (k_x^2 + k_y^2),$$

$$\epsilon(k, q, \mu, b) = \epsilon_0(\mu, b) - D_1(b)a^2q^2 + D_2(b)a^2k^2 + O(a^4q^4) + O(a^4k^4)$$

$$\epsilon_0(\mu, b) = -\mu + \left[\frac{b^2}{2}\epsilon_f - 3t_{d1} - 3t_{f1} - 6t_{d2} - 6t_{f2}b^2 - 4t_{d3} - 4t_{f3}b^2\right],$$

$$D_1(b) = D_2(b) = \left[\frac{t_{d1} + b^2t_{f1}}{2} + 2(t_{d2} + b^2t_{f2}) + 2(t_{d3} + b^2t_{f3})\right],$$

$$\vartheta(k, q, b) = \vartheta_0(b) - B_1(b)a^2q^2 + B_2(b)a^2k^2 + O(a^4q^4) + O(a^4k^4),$$

$$\vartheta_0(b) = \left[-\frac{b^2\epsilon_f}{2} - 6t_{d2} + 6t_{f2}b^2 - 4t_{d3} + 4t_{f3}b^2\right],$$

$$B_1(b) = B_2(b) = \left[\frac{t_{d1} - b^2t_{f1}}{2} + 2(t_{d2} - b^2t_{f2}) + 2(t_{d3} - b^2t_{f3})\right]. \quad (8a)$$

Here  $\sigma_{x,y,z}$  are also the Pauli matrices,  $\sigma_0$  is the  $2 \times 2$  identity matrix. In fact, the Pauli matrices  $\sigma$  and  $\tau$  are acting in the space of bands that give rise to Kramers degeneracy (see Figure 2 below). The Rashba spin-orbit coupling (RSOC) between the  $d$ -electrons may be introduced in the Hamiltonian in (8) for ascertaining effects of the broken inversion symmetry (IS) when  $M \neq 0$ . It would be interesting to see how is it possible to use some topological invariant, e. g., spin Chern number [30], to characterize the quantum spin Hall state with broken TRS and IS. All the functions appearing in Eq. (8a) are to be used in Appendix A. Upon dropping the last

term in (8), we find that the Hamiltonian (8), in the basis  $(d_{k,\uparrow}^\dagger \ bc_{k,\downarrow}^\dagger \ d_{k,\downarrow}^\dagger \ bc_{k,\uparrow}^\dagger)^\top$ , could be written as

$$h_{\text{surface}}(k, q, \mu, b, M) = (\epsilon(k, q, \mu, b))\sigma_0 \otimes \tau_0 + \vartheta(k, q, b)\sigma_0 \otimes \tau_z + A_1 a k_x \sigma_z \otimes \tau_x \\ + A_1 a k_y \sigma_z \otimes \tau_y + M \sigma_z \otimes \tau_z \quad (9)$$

$$h_{\text{surface}}(k, q, \mu, b, M) = \begin{pmatrix} \mathfrak{h}_+ = \mathfrak{h}(k_x, k_y, q, \mu, b, M) & 0 \\ 0 & \mathfrak{h}_- = \mathfrak{h}^*(-k_x, -k_y, q, \mu, b, -M) \end{pmatrix} \quad (10)$$

where  $\mathfrak{h}_\pm = (\epsilon(k, q, \mu, b))\tau_0 + \mathbf{n}(k_x, k_y, q, b) \cdot \boldsymbol{\tau} + M\tau_z$ , the two blocks  $(\mathfrak{h}_+, \mathfrak{h}_-)$ , characterized by the pseudo-spin indices  $(+, -)$ , are related to each other by time reversal symmetry (TRS) for  $M = 0$ , and  $\mathbf{n}(k_x, k_y, q, b) = (A_1 a k_x, A_1 a k_y, \vartheta(k_x, k_y, q, b))$ . On a quick side note, it is worth mentioning that  $h_{\text{surface}}(k, q, \mu, b, M = 0)$  corresponds to Qi-Wu-Zhang (QWZ) model[31-33]. As shown by these authors, the situation corresponds to the QSH state, for the spin Hall conductance of  $\mathfrak{h}(k_x, k_y, q, \mu, b, M = 0)$  and  $\mathfrak{h}^*(-k_x, -k_y, q, \mu, b, -M = 0)$  are not zero but the net Hall conductance of the system described by Eq.(10) is zero. A twisted Hilbert space is the important feature of a strong topological insulator. We show below that the Hilbert space of our system is twisted. The appearance of topologically-protected surface states is the physical consequence of this nontriviality.

### 3. $Z_2$ Invariant using the Eigenvalues of the Space Inversion Operator

For the purpose stated above, following Fu and Kane [13], the  $Z_2$  invariant using the eigenvalues of the parity operator needs to be calculated. The objective could be accomplished with relative ease if the Hamiltonian in (8) is written down in the Dirac basis similar to the Bernevig–Hughes–Zhang (BHZ) model [34] presented over a decade and half ago for quantum wells. We write the Hamiltonian in (8) as

$$h_{\text{surface}} = \begin{pmatrix} \mathfrak{h}_+ & \mathcal{L}_1 \\ \mathcal{L}_2 & \mathfrak{h}_- \end{pmatrix}, \quad \mathcal{L}_1 = \begin{pmatrix} 0 & -iA_1 a q \\ -iA_1 a q & 0 \end{pmatrix}, \quad \mathcal{L}_2 = \begin{pmatrix} 0 & iA_1 a q \\ iA_1 a q & 0 \end{pmatrix}, \quad (11)$$

where  $ak_\mp = ak_x \mp iak_y$ . The interblock coupling is incorporated by the matrices  $(\mathcal{L}_1, \mathcal{L}_2 = \mathcal{L}_1^\dagger)$ . We now write the Hamiltonian in (11) in Dirac basis similar to the BHZ model: In terms of the column vector  $(d_{k,\uparrow}^\dagger \ d_{k,\downarrow}^\dagger \ bc_{k,\uparrow}^\dagger \ bc_{k,\downarrow}^\dagger)^\top$ , we have

$$h_{\text{surface}}^{BHZ}(k, q, \mu, b, M) = \frac{\epsilon_d + \epsilon_c}{2} I^{4 \times 4} + \sum_{a=0,1,2,3,5} d_a(k, q, \mu, b) \gamma^a + M \sigma_0 \otimes \tau_z \quad (12)$$

where  $d_0 = \frac{\epsilon_d - \epsilon_c}{2}$ ,  $\epsilon_d = (\epsilon(k, q, \mu, b) + \vartheta(k, q, b))$ ,  $\epsilon_c = (\epsilon(k, q, \mu, b) - \vartheta(k, q, b))$ ,  $d_1 = -iA_1 a k_y$ ,  $d_2 = iA_1 a k_x$ ,  $d_3 = A_1 a \chi$ , and  $d_5 = 0$ . The Hamiltonian  $h_{\text{surface}}^{BHZ}(k, q, \mu, b, M = 0)$



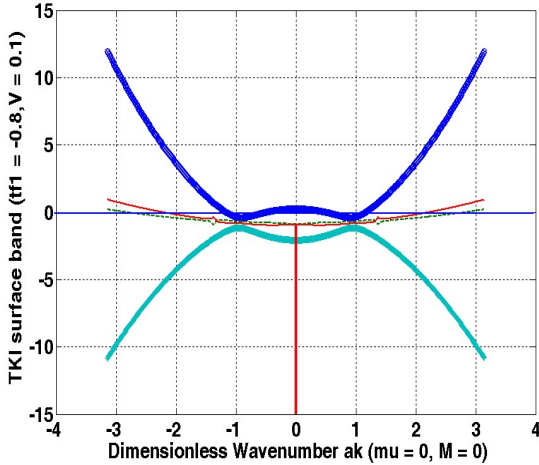
corresponds to the periodic Anderson Hamiltonian (PAM) in the long wavelength limit for the special case  $M = 0$ . The Dirac matrices ( $\gamma^0, \gamma^1, \gamma^2, \gamma^3, \gamma^5$ ) in contravariant notations are  $\gamma^0 = \sigma^z \otimes I^{2 \times 2}$ ,  $\gamma^j = i\sigma^y \otimes \tau^j, j = 1, 2, 3$ , and  $\gamma^5 = i\gamma^0 \gamma^1 \gamma^2 \gamma^3$ . The eigenvalues  $\epsilon_j$  of the Hamiltonian matrix (12) are given by the quartic

$$\epsilon_j^4 + a \epsilon_j^3 + b \epsilon_j^2 + c \epsilon_j + d = 0. \quad (13)$$

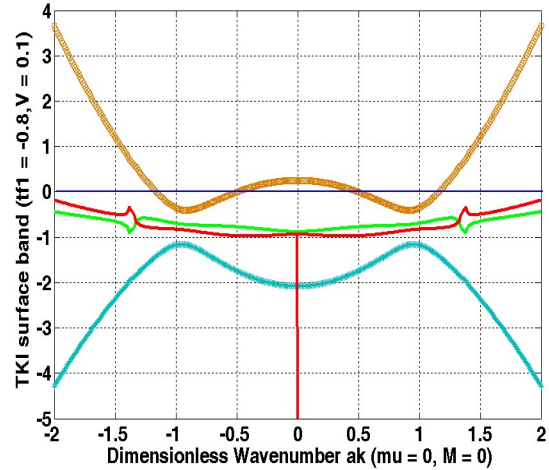
The coefficients ( $a, b, c, d$ ) are given in Appendix A (see Eq. (A.1) -- (A.8)). In view of the Ferrari's solution of a quartic equation, we find the roots as

$$\epsilon_j(s, \sigma, k, b, M) = \epsilon_{j,k}^{s,\sigma}(b) = \sigma \sqrt{\frac{\eta_0(k)}{2}} - \frac{a}{4} + s \left( b_0(k) - \left( \frac{\eta_0(k)}{2} \right) + \sigma c_0(k) \sqrt{\frac{2}{\eta_0(k)}} \right)^{\frac{1}{2}}, \quad (14)$$

where  $j = 1, 2, 3, 4$ ,  $\sigma = \pm 1$  is the spin index and  $s = \pm 1$  is the band-index. Here  $\epsilon_{j,k}^{s,\sigma}(b)$  is simply a short-hand notation. The spin-down ( $\sigma = -1$ ) conduction band ( $s = +1$ ) and the spin-up ( $\sigma = +1$ ) valence band ( $s = -1$ ), denoted respectively by  $\epsilon_1(s = +1, \sigma = -1, k, b)$  and  $\epsilon_2(s = -1, \sigma = +1, k, b)$ , are of primary interest as will be shown below. The functions appearing in Eq. (14) are given in Appendix A. The eigenstates linked to the eigenvalues in  $\epsilon_j(s, \sigma, k, q, \mu, b)$  in (14) are also presented in Appendix B. We have plotted the surface state energy spectra (SSES) given by Eq. (14) as function of the dimensionless wave vector  $ak$  in Figures 2(a) and 2(b). Since the conduction bands are partially empty, the surface state will be metallic. These figures correspond to unbroken TRS ( $M = 0$ ). It will be shown below, calculating the  $Z_2$  invariant using the eigenvalues of the space inversion operator, that the figures correspond



(a)



(b)

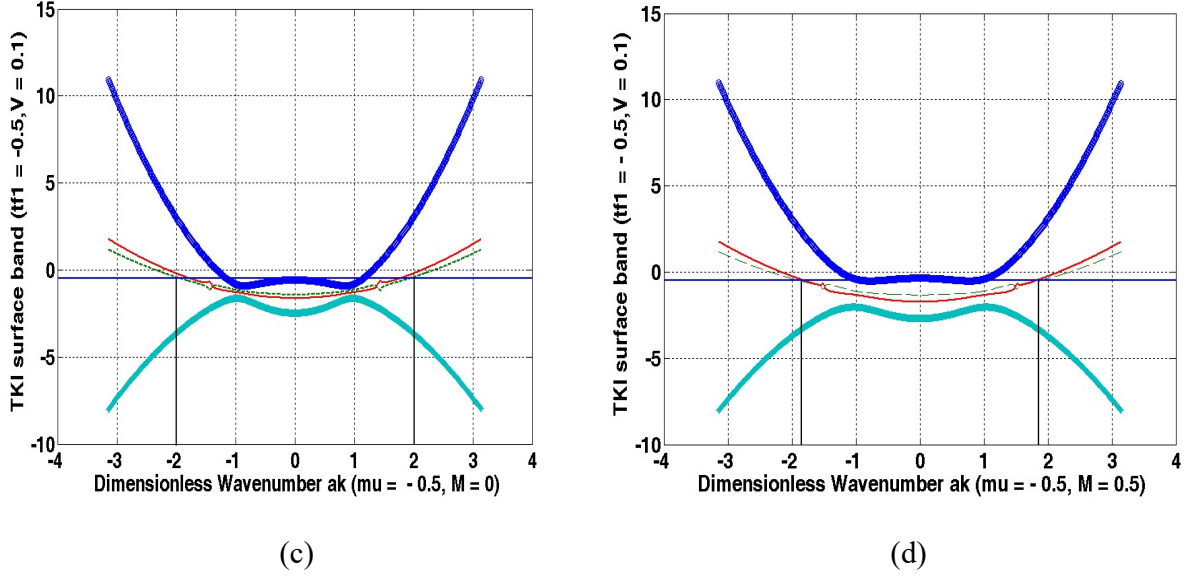
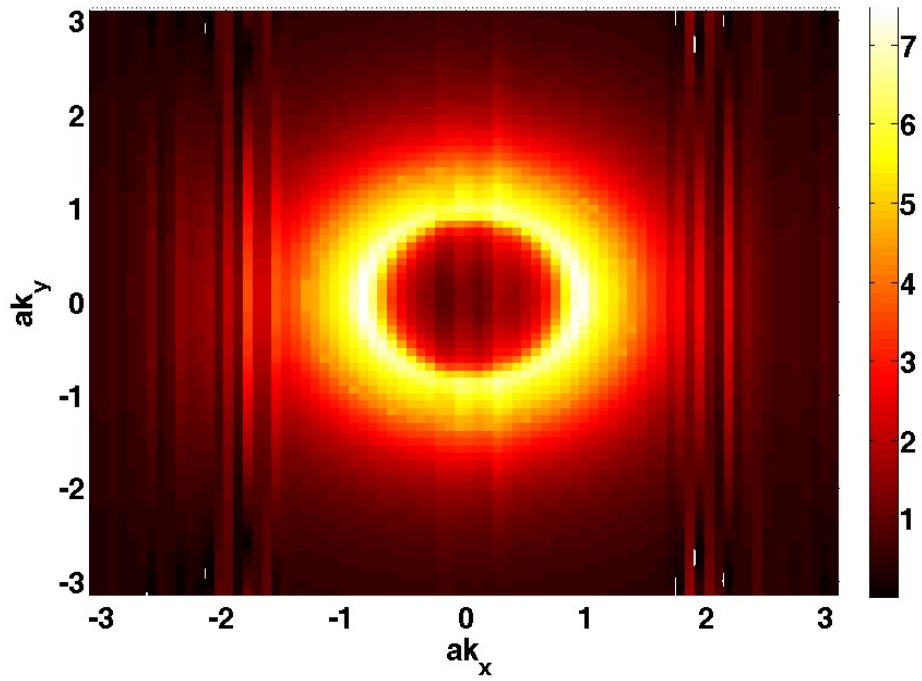


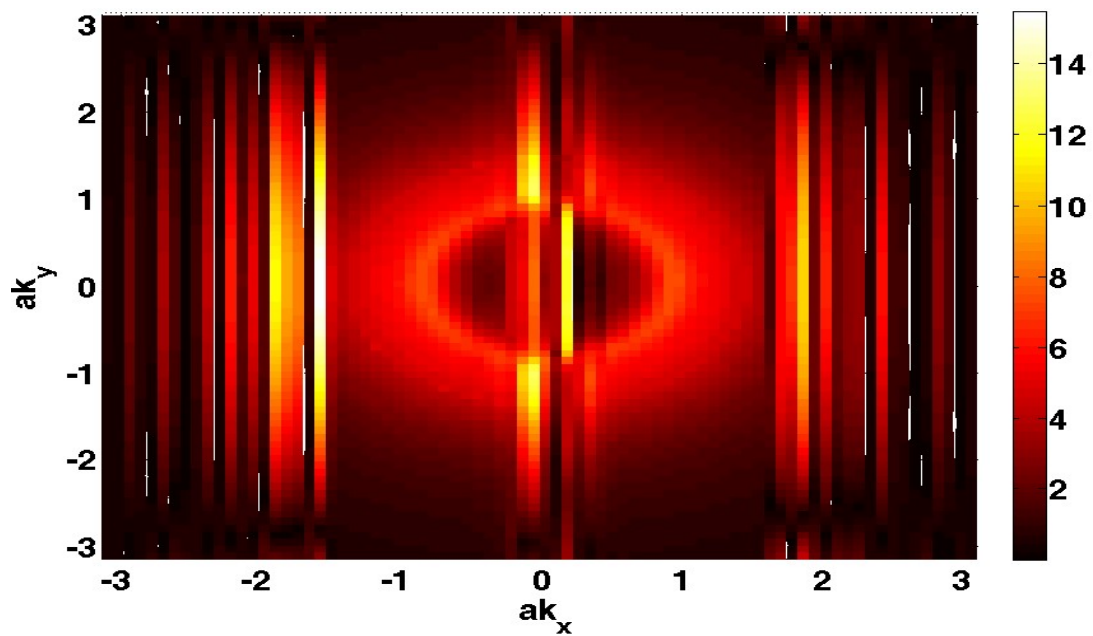
**Figure 2.** The plots of surface state energy spectrum given by Equation (14) as a function of the dimensionless wave vector  $ak$ . The numerical values of the parameters used in the plots are  $t_{d_1} = 1$ ,  $t_{f_1} = (-0.8, -0.5)$ ,  $t_{d_2} = 0.01$ ,  $t_{f_2} = 0.01$ ,  $t_{d_3} = 0.001$ ,  $t_{f_3} = 0.001$ ,  $\epsilon_f = -0.02$ ,  $V = 0.1$ ,  $b = 0.98$ ,  $\mu = (0, -0.5)$ ,  $M = (0, 0.5)$  and  $U_f \gg t_{d_1}$ . The horizontal solid line represents the Fermi energy. Since the conduction bands are partially empty, the surface state will be metallic in all the cases. In (a)-(c), the system is TR symmetric. The energy bands of the system come in Kramers pairs. We observe a Dirac cone like feature in Figures (a) and (b). In Figure (d), TR symmetry is lacking and therefore no Kramers pair is possible.

to QSH phase. There should be a surface Dirac cone (or at least a Kramers degeneracy) at  $k=0$ , as in ref. [35]. We indeed observe a Dirac cone like feature here (see Figure 2(a) and 2(b)) in a certain parameter-window. The numerical values of the parameters used in the plots are  $t_{d_1} = 1$ ,  $t_{f_1} = -0.8$ ,  $t_{d_2} = 0.01$ ,  $t_{f_2} = 0.01$ ,  $t_{d_3} = 0.001$ ,  $t_{f_3} = 0.001$ ,  $\epsilon_f = -0.02$ ,  $V = 0.1$ ,  $b = 0.98$ ,  $\mu = 0$ ,  $M = 0, 0.3$  and  $U_f \gg t_{d_1}$ . In both the figures,  $t_{f_1}$  is negative and, therefore, the figures correspond to the insulating bulk. It may be noted that one needs  $t_{f_1} \sim t_{d_1}$  to access the Dirac-cone feature. The Dirac-cone feature of SSES agrees with several experimental observations reported earlier, such as those by scanning-tunneling microscopy [36,37], angle-resolved photoemission spectroscopy (ARPES)[38,39] and the circular dichroism ARPES[40], and so on. Here, the red curve corresponds to the spin-up valence band  $\epsilon_3$  ( $s = -1, \sigma = +1, k, b$ ), and the green curve to spin-down conduction band  $\epsilon_2$  ( $s = +1, \sigma = -1, k, b$ ). The curves display the band-inversion close to the Fermi energy represented by the horizontal solid line. In Figure 2(c), though  $M = 0$ ,  $\mu \neq 0$ . We observe that the states corresponding to momenta  $ak = (\pm 2, 0)$  or  $(0, \pm 2)$  in Figure 2(a) are degenerate. Furthermore, they satisfy the condition  $ak + aG = -ak$  where  $aG$  is a reciprocal lattice vector. For example, for  $ak = (\pm 2, 0)$  and  $aG = (\mp 4, 0)$ . Of course, there are other possibilities too, for example  $ak = (\pm\sqrt{2}, \pm\sqrt{2})$ . These possibilities we are not taking into account for the simple reason that they do not satisfy the condition  $k +$

$\mathbf{G} = -\mathbf{k}$ . In Figure 2(d),  $M \neq 0$  and therefore TRS is broken. There is no Kramers degeneracy as could be seen in this figure. The figure 2(d) corresponds to QAH as is shown below.



(a)



(b)

**Figure 3.** The contour plots of the Berry-curvature in the z-direction for  $M= 0.08$  as a function of the dimensionless wave vector components  $ak_x$  and  $ak_y$ . The numerical values of the parameters used in the plots are  $t_{d_1} = 1, t_{d_2} = 0.01, t_{f_2} = 0.01, t_{d_3} = 0.001, t_{f_3} = 0.001, \epsilon_f = -0.02, V = 0.1, b = 0.98, \mu = 0,$  and  $U_f \gg t_{d_1}$ . The parameter  $t_{f_1} = -0.8$  in Figure (a), whereas  $t_{f_1} = -0.6$  in Figure (b).

In Figure 3 we have shown the contour plots of the Berry-curvature(BC) in the z-direction for  $M \neq 0$ . The numerical values of the parameters used in the plots are  $t_{d_1} = 1, t_{d_2} = 0.01, t_{f_2} = 0.01, t_{d_3} = 0.001, t_{f_3} = 0.001, \epsilon_f = -0.02, V = 0.1, b = 0.98, \mu = 0,$  and  $U_f \gg t_{d_1}$ . The parameter  $t_{f_1} = -0.8$  in Figure (a) whereas  $t_{f_1} = -0.6$  in Figure (b). Upon integrating BC on a k-mesh-grid of the Brillouin zone (BZ), we calculate the intrinsic anomalous Hall conductivity  $\sigma_{AH}$ (AHC). This yields the Chern number ( $C$ ). A brief outline of the procedure followed is given below in Appendix D. We find that AHC is  $\sigma_{AH} = 1.0471 \left(\frac{e^2}{h}\right)$  (in the former case ( $C = 1.0471$  is close to the integer value 1), while in the latter case it is  $\sigma_{AH} = 1.6607 \left(\frac{e^2}{h}\right)$ ). Furthermore, we found that while for  $t_{f_1} = -0.4, C = 3.3906,$  for  $t_{f_1} = -0.2, C = 3.2181$ . Our conjecture for not obtaining integer values of Chern number leans upon the following: The Hall conductivity  $\sigma_{AH}$  cannot be determined as such from the 2D Dirac model since Eq. (D.1) (see Appendix D) requires an integral over the whole BZ. The integral is outside the Dirac model's range of validity. To circumvent the problem one may possibly choose a momentum space cut-off small compared to the size of BZ and large enough to capture nearly all the contributions to BC integral. This will be within the range of validity of the 2D Dirac model.

Let us now note that the Fermi energy inside the gap intersects the surface state bands in the same BZ, in general, either an even or an odd pair number of times. If there are odd numbers of pair intersections, which guarantees the time reversal invariance, the surface state is topologically non-trivial (strong topological insulator), for moderate disorder (*disorder potential*  $\ll t_{d_1}$ ) cannot remove pairs of such pair-surface-state crossings (SSC). Furthermore, it is also evident that the number of TRIM pair involved in SSC is one (odd). However, when there are an even number of pair-surface-state crossings, the surface states are topologically trivial (weak TI or ordinary Bloch insulators that are topologically equivalent to the filled shell atomic insulator). The quantized topological numbers, the Kane–Mele index  $Z_2$  for QSH phase and the Chern number  $C$  for QAH phase, strongly support such topological states. The QSH band structures are characterized by the topological invariant  $\nu_0 = 0$  ( $Z_2 = +1$ ) and  $\nu_0 = 1$  ( $Z_2 = -1$ ). The former corresponds to weak TI, while the latter to strong TI. In fact, materials with band structures with  $Z_2 = -1$  are expected to exist in systems with strong spin-orbit coupling acting as an internal quantizing magnetic field on the electron system. The graphical representations in Figure 2 (except Figure 2(d)) indicate that the system considered here is a strong TI for  $M = 0$ . If the indication is corroborated by analysis given below, the TKI surface comprises of ‘helical liquids’ which (helicity) is one of the most unique properties of a topologically protected surface state.

In a bid to examine the possibility of helical spin liquids ( equivalently, to calculate the  $Z_2$  invariant using the eigenvalues of the space inversion operator), we note that the  $f$ - and  $d$ -states

have different parities, the inversion symmetry(IS) operator in this band basis is constructed as  $\Pi = I^{2 \times 2} \otimes \tau^z$ . The time reversal (TR) operator for a spin 1/2 particle is  $\Theta = I^{2 \times 2} \otimes \tau^y K$ . The operator  $K$  stands for the complex conjugation. The  $\tau^j$  are Pauli matrices on two-dimensional spin space. The Hamiltonian under consideration, for  $M = 0$ , preserves the time reversal (TRS) and inversion symmetries (IS). It can be easily shown that  $\langle \Theta \psi | \Theta \varphi \rangle = \langle \varphi | \psi \rangle$  taking eigenstate of the z-component of the spin operator  $I^{2 \times 2} \otimes \tau^z$  as the basis. Also,  $\Theta \gamma^0 \Theta^{-1} = \gamma^0$ ,  $\Theta \gamma^5 \Theta^{-1} = \gamma^5$ , and  $\Theta \gamma^j \Theta^{-1} = -\gamma^j$ , where  $j = 1, 2$ , and  $3$ . Similarly,  $\Pi \gamma^0 \Pi^{-1} = \gamma^0$ ,  $\Pi \gamma^j \Pi^{-1} = -\gamma^j$  ( $j = 1, 2$ ), and  $\Pi \gamma^k \Pi^{-1} = \gamma^k$  ( $k = 3, 5$ ). Since only  $\gamma^0$  and  $\gamma^5$  are even under time reversal and inversion (and  $d_5 = 0$ ), at a time reversal invariant momentum (TRIM)  $K_i$  where the system preserves both TR and IS, the Hamiltonian will have the form  $h_{\text{surface}}^{\text{BHZ}}(k = K_i, q, \mu, b, M = 0) = \frac{\epsilon_d + \epsilon_c}{2} I^{4 \times 4} + d_0(k = K_i, q, \mu, b) \gamma^0$ . The eigenvalues of  $\gamma^0$  are  $\pm 1$  (multiplicity 2). The corresponding eigenvectors are  $|+\rangle = (1/\sqrt{2})(1 \ 1 \ 0 \ 0)^T$  and  $|-\rangle = (1/\sqrt{2})(0 \ 0 \ 1 \ 1)^T$ . Here  $\langle + | \gamma^0 | + \rangle = 1$  and  $\langle - | \gamma^0 | - \rangle = -1$ . We obtain

$$\begin{aligned} \langle + | h_{\text{surface}}^{\text{BHZ}}(k = K_i, q, \mu, b, M = 0, W_0) | + \rangle &= \epsilon_d = E_+, \\ \langle - | h_{\text{surface}}^{\text{BHZ}}(k = K_i, q, \mu, b, M = 0, W_0) | - \rangle &= \epsilon_c = E_-. \end{aligned} \quad (15)$$

Here

$$d_0 = \frac{\epsilon_d - \epsilon_c}{2}, \quad \epsilon_d = (\epsilon(k, q, \mu, b) + \vartheta(k, q, b)), \quad \epsilon_c = (\epsilon(k, q, \mu, b) - \vartheta(k, q, b)). \quad (16)$$

Obviously enough, if  $E_- < E_+$ , the state  $|-\rangle$  is occupied and the parity of the state at TRIM  $K_i$  is  $-1$ . In the opposite case ( $E_- > E_+$ ), the state  $|+\rangle$  is occupied and the parity is  $+1$ . Therefore, the parity is given by  $(-sgn[d_0])$ .

At this point we make a digression to obtain the result that the  $Z_2$  invariant can be calculated simply by the parity eigenvalues at TRIMs. The surface states correspond to the eigenstates (or the Bloch states  $|\dot{u}^{(\alpha)}(\mathbf{k})\rangle$ ) linked to the eigenvalues in  $\epsilon_j(s, \sigma, k, b, M = 0)$ . These are presented in Appendices A and B. We consider now a matrix representation of the time reversal (TR) operator  $\Theta$  in the Bloch wave function basis. With  $\alpha$  and  $\beta$  as the band indices we consider the representation is  $\xi_{\alpha\beta}(k) = \langle \dot{u}^{(\alpha)}(-\mathbf{k}) | \Theta | \dot{u}^{(\beta)}(\mathbf{k}) \rangle$ . This matrix relates the two Bloch states  $|\dot{u}^{(\alpha)}(-\mathbf{k})\rangle$  and  $|\dot{u}^{(\beta)}(\mathbf{k})\rangle$  via  $|\dot{u}^{(\alpha)}(-\mathbf{k})\rangle = \sum_{\beta} \xi_{\alpha\beta}^*(k) \Theta | \dot{u}^{(\beta)}(\mathbf{k}) \rangle$ . With the aid of this one can easily show that  $\xi_{\alpha\beta}(k)$  is a unitary matrix ( $\xi^\dagger \xi = I$ ). We also find that it has the property  $\xi_{\alpha\beta}(-k) = -\xi_{\beta\alpha}(k)$ . This implies that the matrix  $\xi_{\alpha\beta}(K_i)$  at a TRIM becomes anti-symmetric, i.e.  $\xi_{\alpha\beta}(K_i) = -\xi_{\beta\alpha}(K_i) \neq 0$ . Only when the bands  $\alpha$  and  $\beta$  form a Kramers pair, such a non-zero  $\xi_{\alpha\beta}$  is obtained. Yet another which we need to consider is the Berry connection matrix defined as  $\gamma_{\alpha\beta}(k) = -i \langle \dot{u}^{(\alpha)}(\mathbf{k}) | \nabla_{\mathbf{k}} | \dot{u}^{(\beta)}(\mathbf{k}) \rangle$ . In view of the results  $\langle \Theta \psi | \Theta \varphi \rangle = \langle \varphi | \psi \rangle$  and  $|\dot{u}^{(\alpha)}(-\mathbf{k})\rangle = \sum_{\beta} \xi_{\alpha\beta}^*(k) \Theta | \dot{u}^{(\beta)}(\mathbf{k}) \rangle$  we arrive at the relation linking  $\gamma_{\alpha\beta}(k)$  and  $\gamma_{\alpha\beta}(-k)$ :

$$\boldsymbol{\gamma}(-\mathbf{k}) = \boldsymbol{\xi}(\mathbf{k})\boldsymbol{\gamma}^*(\mathbf{k})\boldsymbol{\xi}^\dagger(\mathbf{k}) + i\boldsymbol{\xi}(\mathbf{k})\nabla_{\mathbf{k}}\boldsymbol{\xi}^\dagger(\mathbf{k}). \quad (17)$$

Upon taking the trace we find  $\text{tr}(\boldsymbol{\gamma}(-\mathbf{k})) = \text{tr}(\boldsymbol{\gamma}^*(\mathbf{k})) + i \text{tr}(\boldsymbol{\xi}(\mathbf{k})\nabla_{\mathbf{k}}\boldsymbol{\xi}^\dagger(\mathbf{k}))$ . Since  $\gamma_{\beta\alpha} = \gamma_{\alpha\beta}^*$  and  $\boldsymbol{\xi}\nabla\boldsymbol{\xi}^\dagger = -(\nabla\boldsymbol{\xi})\boldsymbol{\xi}^\dagger$ , upon replacing  $-\mathbf{k}$  by  $\mathbf{k}$  in the preceding equation one may write  $\mathbf{A} = \text{tr}(\boldsymbol{\gamma}(\mathbf{k})) = \text{tr}(\boldsymbol{\gamma}(-\mathbf{k})) + i \text{tr}(\boldsymbol{\xi}^\dagger(\mathbf{k})\nabla_{\mathbf{k}}\boldsymbol{\xi}(\mathbf{k}))$ . We shall need this result below. The Berry curvature of  $\text{tr}(\boldsymbol{\gamma}(\mathbf{k}))$  may be defined as  $\boldsymbol{\Omega} = \text{curl}\mathbf{A}$ . Since the system preserves the time reversal (TRS) and inversion symmetries (IS), one may select any gauge which renders  $\mathbf{A}$  equal to zero. We now consider the anti-symmetric and unitary matrix  $\zeta_{\alpha\beta}(k) = \langle \psi^{(\alpha)}(k) | \Pi \Theta | \psi^{(\beta)}(k) \rangle$  (where  $\Pi^2 = 1$ ) to examine the consequence of setting  $\mathbf{A}$  equal to zero. Since we find from ref.[12] that  $\mathbf{A} = \text{tr}(\boldsymbol{\gamma}(\mathbf{k})) = \frac{i}{2} \text{tr}(\zeta^\dagger \nabla_{\mathbf{k}} \zeta) = \frac{i}{2} \nabla_{\mathbf{k}} \text{tr}(\log \zeta) = i \nabla_{\mathbf{k}} \log(\sqrt{\det[\zeta]})$ , it is clear that in order to make  $\mathbf{A} = 0$ , one needs to adjust the phase of Bloch states  $|\psi^{(\alpha)}(k)\rangle$  such that  $\text{Pf}(\zeta) = 1$ . Suppose now  $\rho(K_i^{\text{trim}}) = \pm 1$  are the eigenvalues of  $\Pi$  for band  $\alpha$  at TRIM  $K_i^{\text{trim}}$ , one obtains the matrix

$$\xi_{\alpha\beta}(K_i^{\text{trim}}) = \langle \psi^{(\alpha)}(-K_i^{\text{trim}}) | \Pi \Theta | \psi^{(\beta)}(K_i^{\text{trim}}) \rangle = \zeta_{\alpha\beta}(K_i^{\text{trim}}) \rho_{\alpha}(K_i^{\text{trim}}). \quad (18)$$

Obviously enough, when  $\rho_{\alpha} = \rho_{\beta}$ ,  $\xi_{\alpha\beta}(K_i) = -\xi_{\beta\alpha}(K_i) \neq 0$ . Only when the bands  $\alpha$  and  $\beta$  form a Kramers pair, such a non-zero  $\xi_{\alpha\beta}$  is obtained. It follows that if the bands  $\alpha$  and  $\beta$  are the  $n$ th Kramers pair in the total of  $2N$  bands, we may write  $\rho_{\alpha} = \rho_{\beta} \equiv \rho_{2n}$ . From Eq.(17), one can now see that  $\text{Pf}[\xi_{\alpha\beta}(K_i^{\text{trim}})] = \text{Pf}[\zeta_{\alpha\beta}(K_i^{\text{trim}})] \prod_{n=1}^N \rho_{2n}(K_i^{\text{trim}})$ . Since  $\text{Pf}(\zeta) = 1$ , in view of this result and Eq.(C.3) in appendix C, we find that that the  $Z_2$  invariant can be calculated simply by the parity eigenvalues  $\rho_{2n}$  at TRIMs  $K_i^{\text{trim}}$ , that is  $(-1)^{\nu} = \prod_i \delta(K_{\text{trim}}^{(i)}) = \prod_i \prod_n \rho_{2n}(K_{\text{trim}}^{(i)})$ . Upon getting back to Eq.(16) and taking into account the observations below this equation, the parity of the occupied state at  $K_{\text{trim}}^{(i)}$ , viz.  $\delta(K_{\text{trim}}^{(i)})$ , is given by  $\delta(K_{\text{trim}}^{(i)}) = (-\text{sgn}[d_0])$ . Besides, from Eq. (8a), it is easy to infer  $\epsilon_c > \epsilon_d$  at a given momentum. This implies that  $E_- > E_+$ . Regarding the topology of our band system, this in turn leads to the conclusion that  $\nu = 1$ . This means that the system is a strong topological (non-trivial) insulator.

#### 4. Floquet Theory

The original time-dependent problem (with periodicity in external driving force) could be mapped into effective time-independent formulation in Floquet theory [41]. The theory was used extensively in the past in the theoretical studies of external driving on transport in various systems commissioning combination of the theory with Schrodinger equation [42], Green's functions [43-45], quantum master equation [46,47], scattering matrix approach [48], and so on. The combinations of the Floquet theory with dynamical mean field theory [49], and slave boson protocol [50] were also formulated for strongly correlated systems. Our approach is in acquiescence to the latter. We assume the normal incidence of CPOF on the surface  $\text{SmB}_6$  with the thickness  $d = 30 \text{ nm}$ . Suppose the angular frequency of the optical field incident on the film is

$\omega \approx 10^{15} \text{radian} - \text{s}^{-1}$  and wavelength  $\lambda_{in} \approx 1500 \text{ nm}$ . Therefore the ratio  $d/\lambda_{in} \approx 0.02 \ll 1$ . Upon taking the field into consideration our Hamiltonian becomes time dependent. The Floquet theory can be applied to our time-periodic Hamiltonian  $H_{surface}(t) = H_{surface}(t + T)$  with the period  $T = 2\pi/\omega$ . Analogous to the Bloch theory involving quasi-momentum, a solution  $|\eta(t)\rangle = \exp(-i\hat{\epsilon}t) |\xi(t)\rangle$  involving the Floquet quasi-energy  $\hat{\epsilon}$  could be written down for the time-dependent Schrodinger equation of the system. The Floquet state satisfies  $|\xi(t)\rangle = |\xi(t + T)\rangle$  and, therefore, could be expanded in a Fourier series  $|\xi(t)\rangle = \sum_r \exp(-ir\omega t) |\xi_r\rangle$  where  $r$  is an integer. Then the wave function, in terms of the quasi-energy  $\hat{\epsilon}$  has the form  $|\eta(t)\rangle = \sum_r \exp\left(-i\left(\frac{\hat{\epsilon}}{\hbar} + r\omega\right)t\right) |\xi_r\rangle$ . This makes us arrive at an infinite dimensional eigenvalue equation in the Sambe space (the extended Hilbert space)[26]:

$$\sum_s H_{surface,r,s} |\xi_n^s\rangle = (s\hbar\omega\delta_{r,s} + \frac{1}{T} \int_0^T H_{surface}(t) e^{i(r-s)\omega t} dt) |\xi_n^s\rangle = \hat{\epsilon}_n |\xi_n^s\rangle. \quad (19)$$

The matrix element  $H_{surface,\alpha,\beta}$  is given by  $H_{surface,\alpha,\beta} = \alpha\hbar\omega\delta_{\alpha,\beta} + \frac{1}{T} \int_0^T H_{surface}(t) e^{i(\alpha-\beta)\omega t} dt$ , where  $(\alpha, \beta)$  are integers. This is the Floquet state surface Hamiltonian of the system. One can now write

$$H_{surface,\alpha,\beta} = \begin{pmatrix} \dots & \dots & \dots & \dots & \dots \\ \dots & H_{surface,-1,-1} & H_{surface,-1,0} & H_{surface,-1,1} & \dots \\ \dots & H_{surface,0,-1} & H_{surface,0,0} & H_{surface,0,1} & \dots \\ \dots & H_{surface,1,-1} & H_{surface,1,0} & H_{surface,1,1} & \dots \\ \dots & \dots & \dots & \dots & \dots \end{pmatrix}. \quad (20)$$

The optical field  $\mathbf{E}(t)$  may be expressed in terms of the electric scalar potential (assumed to be zero) and the time-varying magnetic vector potential  $\mathbf{A}(t) = \mathbf{A}(t + T) = \mathbf{A}_1(\sin(\omega t), \sin(\omega t + \psi), 0)$  through the relation:  $\mathbf{E}(t) = -\frac{\partial \mathbf{A}(t)}{\partial t} = -\mathbf{E}(\cos(\omega t), \cos(\omega t + \psi), 0)$ ,  $\mathbf{E} = \mathbf{A}_1\omega$ . In particular, when the phase  $\psi = 0$  or  $\pi$ , the optical field is linearly polarized. When  $\psi = +\pi/2$  ( $\psi = -\pi/2$ ), the optical field is left-handed (right-handed) circularly polarized. Once we have included a gauge field, it is necessary that we make the Peierls substitution  $H_{surface}(t, b) = H_{surface}\left(\mathbf{k} - \frac{e}{\hbar}\mathbf{A}(t), b\right)$ . The quantity  $aA_0 = \frac{aeE}{\hbar\omega}$  corresponds to the light intensity. It is a dimensionless quantity. In view of the Floquet theory [24-29], we can now write a static effective Hamiltonian, in the off-resonant regime using the Floquet-Magnus (high-frequency) expansion [27]:

$$H_{surface}^{Floquet}(k) = H_{surface,0,0} + \frac{[H_{surface,0,-1}, H_{surface,0,1}]}{\hbar\omega} + O(\omega^{-2}), \quad (21)$$

where  $H_{surface,n,m} = \frac{1}{T} \int_0^T H_{surface}(t) e^{i(n-m)\omega t} dt$  with  $n \neq m$ . For  $M = 0$ , as we have seen in the previous section, we obtain QSH state with the net Hall conductance of the system described by Eq.(10) as zero. We now consider the same QSH insulator and write

$$\begin{aligned}
H_{surface,0,0} &= h_{surface}(k, q, \mu, b) + \left[ \frac{t_{d1} + b^2 t_{f1}}{2} + 2(t_{d2} + b^2 t_{f2}) + 2(t_{d3} + b^2 t_{f3}) \right] \\
&\times (a^2 A_0^2) \sigma_0 \otimes \tau_0 + \left[ \frac{t_{d1} - b^2 t_{f1}}{2} + 2(t_{d2} - b^2 t_{f2}) + 2(t_{d3} - b^2 t_{f3}) \right] (a^2 A_0^2) \sigma_0 \otimes \tau_z, \quad (22) \\
H_{surface,0,-1} &= - \left[ \frac{t_{d1} + b^2 t_{f1}}{2} + 2(t_{d2} + b^2 t_{f2}) + 2(t_{d3} + b^2 t_{f3}) \right] ia^2 (k_x + e^{-i\psi} k_y) A_0 \sigma_0 \otimes \tau_0 \\
&- \left[ \frac{t_{d1} - b^2 t_{f1}}{2} + 2(t_{d2} - b^2 t_{f2}) + 2(t_{d3} - b^2 t_{f3}) \right] ia^2 (k_x + e^{-i\psi} k_y) A_0 \sigma_0 \otimes \tau_z \\
&- (i/2) A_1 (aA_0) \sigma_z \otimes \tau_x - (i/2) A_1 (aA_0) e^{-i\psi} \sigma_0 \otimes \tau_y, \quad (23) \\
H_{surface,0,1} &= \left[ \frac{t_{d1} + b^2 t_{f1}}{2} + 2(t_{d2} + b^2 t_{f2}) + 2(t_{d3} + b^2 t_{f3}) \right] ia^2 (k_x + e^{i\psi} k_y) A_0 \sigma_0 \otimes \tau_0 \\
&+ \left[ \frac{t_{d1} - b^2 t_{f1}}{2} + 2(t_{d2} - b^2 t_{f2}) + 2(t_{d3} - b^2 t_{f3}) \right] ia^2 (k_x + e^{-i\psi} k_y) A_0 \sigma_0 \otimes \tau_z \\
&+ (i/2) A_1 (aA_0) \sigma_z \otimes \tau_x + (i/2) A_1 (aA_0) e^{i\psi} \sigma_0 \otimes \tau_y. \quad (24)
\end{aligned}$$

From the action of the time reversal operator on the wave function we see, that it leads to a complex conjugation of the wave function. Thus, in the case of spin-less wave functions as  $\Theta = K$ , where  $K$  is the operator for complex conjugation. More generally, we can write  $\Theta = UK$  where  $U$  is a unitary operator. Furthermore, for a spin-1/2 particle, flipping the spin coincides with the time-reversal. This means  $\Theta \hat{S} = -\hat{S}$  where  $\hat{S} = \frac{1}{2} \hat{\sigma}$  and  $\hat{\sigma}$  is the vector of Pauli matrices. In view of these, one may also choose  $\Theta = i\sigma_y \otimes \tau_0 K$ . Upon making use of the results  $\Theta \hat{A} \Theta^{-1} = \hat{A}$ ,  $\Theta \hat{B} \Theta^{-1} = -\hat{B}$ , and so on, where  $\hat{A} = \sigma_0 \otimes \tau_0$ ,  $\sigma_z \otimes \tau_y$ , ... and  $\hat{B} = \sigma_0 \otimes \tau_y, \dots$ , we find that

$$\begin{aligned}
&\Theta H_{surface}^{Floquet}(ak_x, ak_y) \Theta^{-1} \\
&= H_{surface}^{Floquet}(-ak_x, -ak_y) + (4a^2 A_0^2 \sin\psi / \hbar\omega) \{A_1 ak_x \sigma_0 \otimes \tau_x + A_1 ak_y \sigma_z \otimes \tau_y\} \\
&\times \left[ \frac{t_{d1} + b^2 t_{f1}}{2} + 2(t_{d2} + b^2 t_{f2}) + 2(t_{d3} + b^2 t_{f3}) \right] + \left( \frac{4a^2 A_0^2 A_1^2 \sin\psi}{\hbar\omega} \right) \sigma_z \otimes \tau_z, \quad (25)
\end{aligned}$$

where  $\Theta H_{surface}^{Floquet}(ak_x, ak_y) \Theta^{-1} = H_{surface}^{Floquet}(k)(-ak_x, -ak_y)$  only when  $\psi = 0$  or  $\pi$ , that is, when the optical field is linearly polarized. In this case, the time reversal symmetry (TRS) is not broken. However, when  $\psi \neq 0$  or  $\pi$ , TRS is broken. We now consider the particular cases where  $\psi = +\pi/2$  and  $\psi = -\pi/2$ . For the former the optical field is left-handed circularly polarized,



whereas for the latter it is right-handed. Thus, the (previously not known) consequence is that the incidence of the CPOF on the SmB<sub>6</sub> surface will be able to create a QSH insulator with the broken TRS.

The Hamiltonian to describe this broken TRS system, in the basis  $(d_{k,\uparrow}^\dagger \ bc_{k,\downarrow}^\dagger \ d_{k,\downarrow}^\dagger \ bc_{k,\uparrow}^\dagger)^\top$ , could be written as  $H_{\text{surface}}^{\text{Floquet}}(k) =$

$$\begin{pmatrix} E_1 & A_{10P}^+(ak_-) & 0 & -i A_{10P}^+aq \\ A_{10P}^+(ak_+) & E_2 & -i A_{10P}^+aq & 0 \\ 0 & i A_{10P}^-aq & E_3 & -A_{10P}^-(ak_-) \\ i A_{10P}^-aq & 0 & -A_{10P}^-(ak_+) & E_4 \end{pmatrix} \quad (26)$$

where  $\mathbf{k} = (k_x, k_y)$ ,  $ak_{\mp} = ak_x \mp iak_y$ ,  $E_1 = \epsilon_{OP} + \vartheta_{OP}^+$ ,  $E_2 = \epsilon_{OP} - \vartheta_{OP}^+$ ,  $E_3 = \epsilon_{OP} + \vartheta_{OP}^-$ ,  $E_4 = \epsilon_{OP} - \vartheta_{OP}^-$ ,  $A_{10}^\pm = A_1 \left( 1 \pm 2B_2 \sin\psi \left( \frac{a^2 A_0^2}{\hbar\omega} \right) \right)$ , and  $A_1 = 2Vb$ . The functions  $\epsilon_{OP} = \epsilon_{OP}(k, q, \mu, b)$  and  $\vartheta_{OP}^\pm = \vartheta_{OP}^\pm(k, q, b)$  are defined below:

$$\epsilon_{OP}(k, q, \mu, b) = \epsilon_0(\mu, b) - D_1(b)a^2q^2 + D_2(b)a^2k^2 + a^2A_0^2D_2(b) + O(a^4k^4),$$

$$\vartheta_{OP}^\pm(k, q, b) = \vartheta_0(b) - B_1(b)a^2q^2 + B_2(b)a^2k^2 - \left( a^2A_0^2B_2 \pm \left( \frac{a^2A_0^2}{\hbar\omega} \right) \sin\psi A_1^2 \right). \quad (27)$$

The eigenvalues ( $\epsilon_\alpha$ ) of the matrix (26) is given by the quartic  $\epsilon_\alpha^4 + \gamma_{10P}(k, b) \epsilon_\alpha^3 + \gamma_{20P}(k, b) \epsilon_\alpha^2 + \gamma_{30P}(k, b) \epsilon_\alpha + \gamma_{40P}(k, b) = 0$  ( $\alpha = 1, 2, 3, 4$ ) where the coefficients  $\gamma_{\beta 0P}(k, b)$  ( $\beta = 1, 2, 3, 4$ ) are given by

$$\gamma_{10P}(k, b) = -\sum_{\mu} E_{\mu}, \gamma_{20P}(k, b) = \left( \frac{1}{2} \right) \sum_{\mu \neq \nu} E_{\mu} E_{\nu} - 2(A_{10P}^+ A_{10P}^-)(aq)^2 - (A_{10P}^+)^2 + A_{10P}^-)^2 (ak)^2, \quad (28)$$

$$\gamma_{30P}(k, b) = \left( -\frac{1}{6} \right) \sum_{\mu \neq \nu \neq \sigma} E_{\mu} E_{\nu} E_{\sigma} + (A_{10P}^+ A_{10P}^-)(aq)^2 \sum_{\mu} E_{\mu} + A_{10P}^-)^2 (ak)^2 (E_1 + E_2) +$$

$$A_{10P}^+)^2 (ak)^2 (E_3 + E_4), \quad (29)$$

$$\gamma_{40P}(k) = \prod_{\mu} E_{\mu} - A_{10P}^-)^2 (ak)^2 (E_1 E_2) - A_{10P}^+)^2 (ak)^2 (E_3 E_4) - A_{10P}^+ A_{10P}^- (aq)^2 (E_1 E_4 + E_2 E_3) +$$

$$A_{10P}^-)^2 A_{10P}^+)^2 (ak)^4 + A_{10P}^-)^2 A_{10P}^+)^2 (aq)^4 - 2A_{10P}^-)^2 A_{10P}^+)^2 (aq)^2 ((ak_x)^2 - (ak_y)^2). \quad (30)$$

It may be noted that to denote these eigenvalues we have used the symbol *var epsilon* which is distinct from that in Eq. (13). Once again, in view of the Ferrari's solution of a quartic equation, we find the roots as

$$\varepsilon_\alpha(s, \sigma, k, b) = s \sqrt{\frac{\eta_{OP}(k)}{2} - \frac{\gamma_{1OP}(k,b)}{4}} + l \left( b_{OP}(k) - \frac{(\eta_{OP}(k))}{2} \right) + s c_{OP}(k) \sqrt{\frac{2}{\eta_{OP}(k)}}^{\frac{1}{2}}. \quad (31)$$

where  $\alpha = 1, 2, 3, 4$ ,  $s = \pm 1$  is the spin index and  $l = \pm 1$  is the band-index. The spin-down ( $s = -1$ ) conduction band ( $l = +1$ ) and the spin-up (down) ( $s = \pm 1$ ) valence bands ( $l = -1$ ), denoted respectively by  $\varepsilon_2(l = +1, s = -1, k, b)$ ,  $\varepsilon_3(l = -1, s = +1, k, b)$ , and  $\varepsilon_4(l = -1, s = -1, k, b)$  somewhat peculiar as will be shown below. The functions appearing in Eq. (31) are given by

$$\begin{aligned} \eta_{OP}(k) &= \frac{2b_{OP}(k)}{3} + (\Delta_{OP}(k) - \Delta_{0OP}(k))^{\frac{1}{3}} - (\Delta_{OP}(k) + \Delta_{0OP}(k))^{\frac{1}{3}}, \\ \Delta_{0OP}(k) &= \left( \frac{b_{OP}^3(k)}{27} - \frac{b_{OP}(k)d_{OP}(k)}{3} - c_{OP}^2(k) \right), \\ \Delta_{OP}(k) &= \left( \frac{2}{729} b_{OP}^6 + \frac{4d_{OP}^2 b_{OP}^2}{27} + c_{OP}^4 - \frac{d_{OP} b_{OP}^4}{81} - \frac{2b_{OP}^3}{27} + \frac{2c_{OP}^2 b_{OP} d_{OP}}{3} + \frac{d_{OP}^3}{27} \right)^{1/2}, \\ b_{OP}(k) &= \left\{ \frac{3\gamma_{1OP}(k,b)^2 - 8\gamma_{2OP}(k,b)}{16} \right\}, \quad c_{OP}(k) = \left\{ \frac{-\gamma_{1OP}(k,b)^3 + 4\gamma_{1OP}(k,b)\gamma_{2OP}(k,b) - 8\gamma_{3OP}(k,b)}{32} \right\}, \\ d_{OP}(k) &= \frac{-3\gamma_{1OP}(k,b)^4 + 256\gamma_{4OP}(k,b) - 64\gamma_{1OP}(k,b)\gamma_{3OP}(k,b) + 16\gamma_{1OP}(k,b)^2\gamma_{2OP}(k,b)}{256}. \end{aligned} \quad (32)$$

The eigenvectors corresponding to  $\varepsilon'_\alpha s$  could be calculated in a manner given in the Appendix B. The value of  $a^2 A_0^2$  (dimensionless intensity of the radiation) is taken to be around 0.8 which is good enough for the radiation field of frequency  $\nu \sim 3 \times 10^{14} \text{ Hz}$  under consideration. Moreover,  $\sin\psi = +1$  ( $\sin\psi = -1$  sign) corresponds to the left-handed (right-handed) circularly polarized radiation above. We notice from Eq.(30) that CPOF not only renormalizes  $d$  and  $f$  electron hopping integrals but also does the renormalization of the hybridization parameter(HP).

We have the renormalized hybridization parameters(HP) as  $A_{1OP}^\pm = A_1 \left( 1 \pm 2B_2 \sin\psi \left( \frac{a^2 A_0^2}{\hbar\omega} \right) \right)$ ,

and  $A_1 = 2Vb$ . As  $B_2(b) \approx \left[ \frac{t_{d1} - b^2 t_{f1}}{2} \right] > 0$ , we find that the renormalized HP  $A_{1OP}^+ > A_1$  ( $A_{1OP}^+ < A_1$ ) for the left-handed (right-handed) CPOF. However, the renormalized HP  $A_{1OP}^- < A_1$  ( $A_{1OP}^- > A_1$ ) for the left-handed(right-handed) CPOF. We note that, in principle, when a renormalized parameter is less than  $A_1$ , it is possible that there is a critical intensity of the radiation  $a^2 A_0^2 \approx \frac{(\hbar\omega)}{(t_{d1} - b^2 t_{f1})}$  at a given frequency at which the RHP in question will be zero. This, however, may affect the topological nature of the material. Now the nearest neighbor hopping elements  $t_{d1}$  and  $t_{f1}$  are related to the band masses by  $t_{d1, f1} \approx \frac{\hbar^2}{2m_{d,f} a^2}$ . If one takes for the band masses

$m_d(m_f) = 1.5 m_e$  ( $50 m_e$ ), where  $m_e$  is the rest mass of the electron, then the corresponding values of the hopping matrix elements are  $t_{d1} \approx 150$  meV and  $t_{f1} \approx 4.5$  meV. This yields the critical intensity of the radiation  $a^2 A_0^2 \approx 2.25$  which is roughly three times the intensity value assumed in the graphical representations in Figure 4.

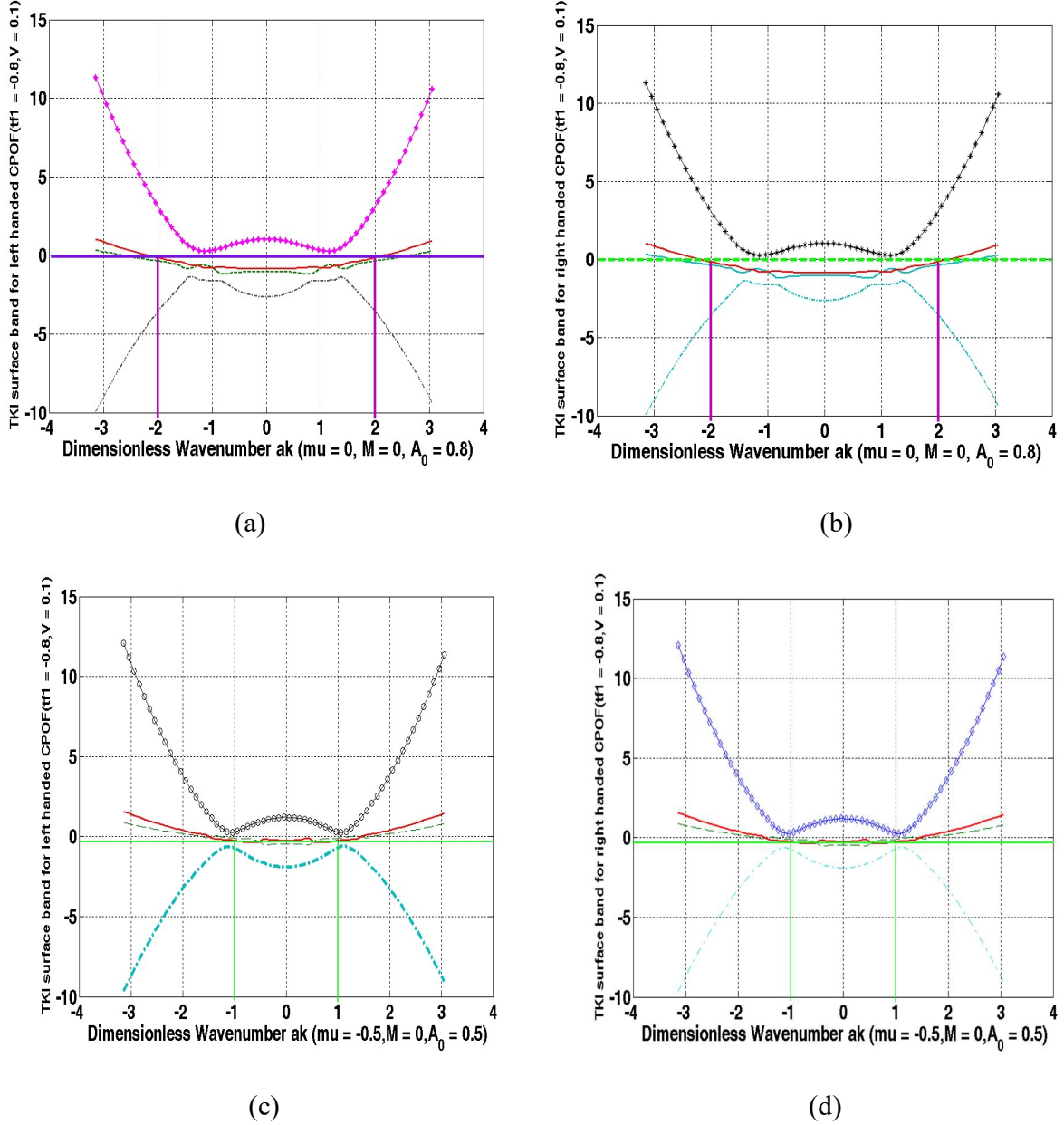


**Figure 4.** The plots of energy eigenvalues  $\varepsilon_a(s, \sigma, k, b)$  in Eq.(31) as a function of  $ak$  for a given intensity of incident radiation  $aA_0 = (0.80, 0.50)$ . The Figures 4(a) and 4(b), respectively, corresponds to the plots for the left handed and the right-handed CPOF. The same is true for the Figures 4(c) and 4(b). The numerical values of the parameters used in the plots in (a) and (b) are  $t_{d1} = 1$ ,  $t_{f1} = -0.8$ ,  $t_{d2} = 0.01$ ,  $t_{f2} = 0.01$ ,  $t_{d3} = 0.001$ ,  $t_{f3} = 0.001$ ,  $\varepsilon_f = -0.02$ ,  $V = 0.1$ ,  $b = 0.98$ ,  $\mu = 0$ ,  $aA_0 = 0.8$ ,  $M = 0$  and  $U_f \gg t_{d1}$ . The numerical values corresponding to (c)

and (d) are  $\mu = -0.5$ , and  $aA_0 = 0.5$  ; the rest of the values are the same as in (a) and (b). The horizontal lines represent the Fermi energy.

In Figure 4 (a), 4(b), 4(c), and 4(d) we have plotted the energy eigenvalues  $\varepsilon_\alpha(s, \sigma, k, b)$  as a function of  $ak$  for  $aA_0 = (0.80, 0.50)$  for the circularly polarized light. Whereas Figures 4(a) and 4(c) correspond to left-handed CPOF, 4(b) and 4(d) to the right-handed CPOF. The numerical values of the parameters used in the plots are  $t_{d_1} = 1$ ,  $t_{f_1} = -0.8$ ,  $t_{d_2} = 0.01$ ,  $t_{f_2} = 0.01$ ,  $t_{d_3} = 0.001$ ,  $t_{f_3} = 0.001$ ,  $\varepsilon_f = -0.02$ ,  $V = 0.1$ ,  $b = 0.98$ ,  $\mu = (0, -0.5)$ ,  $M = 0$  and  $U_f \gg t_{d_1}$ . The horizontal lines represent the Fermi energy. The conduction and valence bands denoted by  $\varepsilon_2(l = +1, s = -1, k, b)$ ,  $\varepsilon_3(l = -1, s = +1, k, b)$ , and  $\varepsilon_4(l = -1, s = -1, k, b)$  represented by differently colored curves, apart from the band-inversion, exhibit some peculiarities by way of the multiple avoided crossings and the near absence of a surface Dirac cone at  $k = 0$  in 4(a) and 4(b) unlike that in Figure 2(a). This non-trivial feature could be ascribed to the interaction of the system with the incident radiation. The figures show that when TRS is broken (though  $M = 0$ ), the emergent novel phase of the system is very robust. The reason being in both the figures the Fermi energy intersects the band  $\varepsilon_3(l = -1, \mu = +1, k, b)$  only in the same BZ an odd pair number of times. This pair of surface state crossings (SSC) corresponds to the momenta  $\mathbf{k} = (\pm 2, 0)$  or  $(0, \pm 2)$  in Figures 4(a) and 4(b). However, in Figures 4(c) and 4(d) the same happens at the momenta  $\mathbf{k} = (\pm 1, 0)$  or  $(0, \pm 1)$ . These momenta satisfy the condition  $a\mathbf{k} + a\mathbf{G} = -a\mathbf{k}$ , where the reciprocal lattice vector  $\mathbf{G}$  is  $(\mp 4, 0)$  or  $(0, \mp 4)$  in Figures 4(a) and 4(b) and  $(\mp 2, 0)$  or  $(0, \mp 2)$  in Figures 4(c) and 4(d). Our graphical representation lead to the fact that, due to the light-matter interaction, the emergent unconventional phase possibly corresponds to QSH. However, as stated in section 1, the conclusive evidence of this TRS-broken phase being QSH/QAH phase will be obtained once we calculate the spin Chern number[30] and the  $Z_2$  invariant which are future tasks.

## 5. Discussion and concluding remarks

As already stated, the strong correlation effects and diverse surface conditions make the GTKI system extremely complicated and almost a Gordian knot. Despite this, as we have seen above, our low-energy model was adequate enough to show that  $\text{SmB}_6$  is a strong TI. It was also able to capture the fact that there should be a surface Dirac cone at  $k=0$  (as in ref.[35]) in Figure 2(a) and 2(b) for  $M = 0$ . For  $M \neq 0$  (Figure 2(d)), since TRS is broken, there is no Kramers degeneracy. By calculating BC and the Chern number we have been able to show that the Figure 2(d) corresponds to QAH state. These are highlights of the present report. In the case of the light-matter interaction in section 4, however, we needed to show that the novel TRS-broken phase corresponds to QSH calculating the spin Chern number[30]. The problem needs an extensive investigation introducing an additional term  $h_z = \left[ \left( \frac{1}{2} \right) \left( \Delta - \alpha_0 \sin(k_y a) \right) \sigma_x \otimes (\tau_z + \tau_0) + \left( \frac{1}{2} \right) \alpha_0 \sin(k_x a) \sigma_y \otimes (\tau_z + \tau_0) \right]$ , which is the Rashba spin-orbit coupling (RSOC) between the  $d$ -electrons, in Eq. (8). The coupling can arise in the present system due to proximity of material lacking in the structural inversion symmetry. In view of the spin-polarized ARPES measurements which appear to confirm the surface helical spin texture [51,52], it would be interesting to see how does surface state react to Rashba splitting as there is evidence of for a

massive surface state at the surface Brillouin zone center which can exhibit Rashba splitting[53]. The Rashba SOC is of particular importance as it is a crucial ingredient for several spintronics and topological phenomena [54]. Moreover, since we have considered surface state quite extensively, a future investigation on the Kondo break down[55,56] is necessary.

There are many other complications to bring home the point that the system needs concerted investigations. In fact, we are presently working on three of the several issues to be discussed below in brief: **(i)**In  $\text{YbB}_{12}$  (a close cousin of  $\text{SmB}_6$ ), a finite residual temperature-linear term in the thermal conductivity  $\kappa/T(T \rightarrow 0)$  is observed demonstrating the presence of gapless and itinerant neutral fermions [57]. On the other hand,  $\kappa/T(T \rightarrow 0)$  in  $\text{SmB}_6$  has been controversial [58,59]. While  $\kappa/T(T \rightarrow 0)$  of  $\text{SmB}_6$  has been reported to be very small but finite [60,61,62], the absence of  $\kappa/T(T \rightarrow 0)$  has been reported in references [61,63]. It is worth mentioning that in ref.[64]  $\kappa/T(T \rightarrow 0)$  has been shown to be finite. **(ii)** In the quantum oscillation (QO) experiments of Li et al. [65], within the bulk hybridization gap, the signatures of two-dimensional Fermi surfaces on (100) and (101) surface planes supporting the presence of topological surface states were obtained. Tan et al. [66] and, subsequently, Hartstein et al. [67], uncovered a deep mystery associated with the insulating bulk of  $\text{SmB}_6$ , which is the formation of a large three-dimensional (solely) conduction electron FS in the absence of the long-range charge transport, given that thus far such FSs have been considered the preserve of metals. The oddity was initially conjectured [68] to be due to the residual density of states at the Fermi energy in  $\text{SmB}_6$ . Later on this was debunked and various theoretical models were put forward that invoke novel itinerant low-energy neutral excitations (majoranas)[69] within the charge gap. These excitations were proposed to produce magneto quantum oscillation (MQO) signals. The theoretical models which entered the fray are based on magnetoexcitons [70], scalar Majorana fermions [71], emergent fractionalized quasiparticles [72, 73] and non-Hermitian states [74]. In the microscopic approach in ref.[73], in particular, it was shown that a repulsive density–density interaction between the  $f$  and  $d$ –electrons representing an attractive interaction between the  $\tilde{f}$ –hole (obtained using a particle-hole transformation involving a fully antisymmetric tensor) and the  $d$ –electron leads to the formation of electrically neutral fermionic quasiparticle conglomerate referred to as the ‘composite exciton Fermi liquid (CEFL)’. The liquid, with electrically neutral bulk, hosts a three dimensional, stable Fermi surface of CEFL induced by an emergent U(1) gauge field. It shares this property with the ground state of the mixed valence compound  $\text{SmB}_6$ . As has been reported earlier [70], in  $\text{SmB}_6$ , the QOs are observed only in the magnetization (de Haas-van Alphen(dHvA)effect). The dHvA oscillations strongly deviate below 1 K from the Lifshitz-Kosevich theory (LKT), which is based on Fermi liquid theory(FLT)[75]. This puts a question mark on any work on  $\text{SmB}_6$  leaning on FLT. An example of this kind is the work of LaBarre et al.[76]. The authors include the contribution from phonons as well as the electronic contribution to the total specific heat  $C(T)$ . Invoking the fact that the large variation in  $C(T)$  among different samples [77-80], the authors [76] implicitly contend that it is entirely plausible that the thermal conductivity is also plagued by sample quality uncertainty. We do agree that the rare-earth purification is exceedingly difficult. Coming back to the issue of NFL, as pointed out

in ref.[69], the elusive particle majoranas plus conduction electrons lead to topological Kondo effect which in turn to non-Fermi liquid (NFL) Kondo physics (non-integer power law for the conductance). This is similar to the conduction electrons plus quantum spins with degenerate levels lead to Kondo effect. It must be mentioned that the QOs in  $\text{YbB}_{12}$  are observed in both magnetization (the de Haas-van Alphen, dHvA, effect) and resistivity (the Shubnikov-de Haas, SdH, effect) at applied magnetic fields  $H$  where the hybridization gap is still finite. The temperature-dependence of the oscillation amplitude complies with the expectations of Fermi-liquid theory [81]. (iii)The Kondo insulating scale in  $\text{SmB}_6$  is extremely vulnerable against even a moderate degree of disorder [82,83]. It is well-known [84-86] that research into the role of impurities in  $\text{SmB}_6$  spans over 40 years. In fact, these impurities form defects in the coherent Kondo lattice. These are so called “Kondo holes.” Theoretical studies propose non-trivial electronic states in the vicinity of the Kondo holes [87]. In fact, doping Gd, La, etc. as Kondo holes into  $\text{SmB}_6$  produces an approximately T-independent Sommerfeld coefficient and increased susceptibility [88]. Abele et al. [89] have argued that the in-gap impurity states form for exceptionally small values of the impurity potential comparable to the hybridization gap which may explain why TKI are found to be exceptionally sensitive to impurities.

An important issue is that the Hermiticity of an open system is universally lost, as the system always involves certain degrees of gain and loss. The ubiquitous electron-electron, electron-impurity, and electron-photon scatterings in an electronic system are responsible for this loss/gain. They lead to complex self-energies  $\Sigma(k, \omega)$  of single electron states such that the lifetime of a single electron state is always finite. As a consequence, the effective single-particle Hamiltonian of Bloch electron in the periodic potential becomes complex. A fundamental difference between Hermitian and non-Hermitian Hamiltonians is that its linearly independent eigenstates do not span the full Hilbert space. This leads to the possibility that the effective quasiparticle Hamiltonian becomes non-diagonalizable at certain momentum, called “exceptional points”. In two and higher dimensions, the exceptional points are characterized by a nontrivial topological index [90]. There has been a growing interest on this issue [91,92]. These considerations are motivation enough to investigate intensively a non-Hermitian GTKI Hamiltonian.

There are other contentious issues too. It is hoped that the details of the problematic issues given above, related/unrelated to the present communication, will motivate the condensed matter physics community to delve deeper into this problem.

In conclusion, looking at the controversies and the possibilities, it is anybody’s guess that there are many unsettled issues. Unless other TKI candidates are discovered and thoroughly studied, it is perhaps difficult to achieve enhancement in the current understanding of strongly correlated topological insulators. In this backdrop, it is pertinent to make an attempt to investigate thoroughly what exactly are the physical explanation of the issues involved. In a future communication, as we already stated, we undertake a part of this demanding task.

## References

- 1 D. J. Kim, S. Thomas.; T. Grant, J. Botimer, Z. Fisk, J. Xia, Sci. Rep., 3, 3150(2013).
- 2 .M.Dzero, K Sun, V. Galitski, P. Coleman, Phys. Rev. Lett. 2010, 104, 106408(2010); *ibid* Rev. B 2012, 85, 045130 (2012).
- 3.Udai Prakash Tyagi, Kakoli Bera and Partha Goswami, On Strong  $f$ -Electron Localization Effect in a Topological Kondo Insulator, *Symmetry*,13(12), 2245 (2021); <https://doi.org/10.3390/sym13122245>.
4. S. Wolgast, C. Kurdak, K. Sun, J. W. Allen, D.-J. Kim, and Z. Fisk, Phys. Rev. B 88, 180405 (2013).
5. X. Zhang, N. P. Butch, P. Syers, S. Ziemak, R. L. Greene, and J. Paglione, Phys. Rev. X 3, 011011 (2013).
6. D. J. Kim, J. Xia, and Z. Fisk, Nat. Mater. 13, 466 (2014).
7. Tran, F.; Blaha, P., Phys. Rev. Lett. 2009, 102, 226401; A. P. Sakhya and K.B. Maiti , Scientific Reports volume 10, Article number: 1262 (2020).
8. N. Wakeham, P. F. S. Rosa, Y. Q. Wang, M. Kang, Z. Fisk, F. Ronning, and J. D. Thompson, Phys. Rev. B 94, 035127 (2016).
9. P. K. Biswas, M. Legner, G. Balakrishnan, M. C. Hatnean, M. R. Lees, D. M. Paul, E. Pomjakushina, T. Prokscha, A. Suter, T. Neupert, et al., Phys. Rev. B 95, 020410 (2017).
- 10..M. Legner, Topological Kondo insulators: materials at the interface of topology and strong correlations(Doctoral Thesis),ETH Zurich Research Collection(2016).Link:<https://www.research-collection.ethz.ch/bitstream/handle/20.500.11850/155932/eth-49918-02.pdf?isAllowed=y&sequence=2>.
11. A. Sharma, H. Yan, L. Zhang, X. Sun X. B. Liu, Y. Lu Y. Highly enhanced many-body interactions in anisotropic 2D semiconductors. *Accounts of Chemical Research*. 2018;51(5):1164–1173. doi: 10.1021/acs.accounts.7b00504.
12. L. Fu, C.L. Kane.: Time reversal polarization and a  $Z_2$  adiabatic spin pump. Phys. Rev. B 74, 195312 (2006); L. Fu, C. L. Kane, and E.J. Mele: Topological insulators in three dimensions. Phys. Rev. Lett. 98, 106803 (2007); C. L. Kane, and E.J. Mele:  $Z_2$  Topological Order and the Quantum Spin Hall Effect. Phys. Rev. Lett. 95, 146802 (2005).
13. A. Amorese, O. Stockert, K. Kummer, N. B. Brookes, Dae-Jeong Kim, Z. Fisk, M. W. Haverkort, P. Thalmeier, L. Hao Tjeng, and A. Severing, Phys. Rev. B 100, 241107(R) (2019).
14. S. Sajad Dabiri, Hosein Cheraghchi, Ali Sadeghi, Light-induced topological phases in thin films of magnetically doped topological insulators Physical Review B 103, 205130 (2021); Haowei Xu, Jian Zhou, Ju Li, Light-induced quantum anomalous Hall effect on the 2D surfaces of 3D topological insulators, Advanced Science, 2101508 (2021).
15. W. Zhu, M. Umer, and J. Gong, Phys. Rev. Research 3, L032026 (2021).
16. L. Zhou, C. Chen, and J. Gong, Phys. Rev. B 94, 075443 (2016).
17. H. Hubener, M. A. Sentef, U. De Giovannini, A. F. Kemper, and A. Rubio, Nat. Commun. 8, 13940 (2017).
18. D. Zhang, H. Wang, J. Ruan, G. Yao, and H. Zhang, Phys. Rev. B 97, 195139 (2018).
19. H. Liu, J.-T. Sun, and S. Meng, Phys. Rev. B 99, 075121 (2019).
20. L. Li, C. H. Lee, and J. Gong, Phys. Rev. Lett. 121, 036401 (2018).

21. X. Liu, P. Tang, H. Hübener, U. De Giovannini, W. Duan, and A. Rubio, arXiv preprint arXiv:2106.06977 (2021).
22. F. Qin, R. Chen, and H.-Z. Lu, *J. Phys. Condens. Matter* **34**, 225001 (2022).
23. J. W. McIver, B. Schulte, F.-U. Stein, T. Matsuyama, G. Jotzu, G. Meier, and A. Cavalleri, Light-induced anomalous hall effect in graphene, *Nature Physics* **16**, 38 (2019).
24. B. K. Wintersperger, C. Braun, F. N. Unal, A. Eckardt, M. D. Liberto, N. Goldman, I. Bloch, and M. Aidelsburger, Realization of an anomalous floquet topological system with ultracold atoms, *Nature Physics* **16**, 1058 (2020).
25. C. S. Afzal, T. J. Zimmerling, Y. Ren, D. Perron, and V. Van, Realization of anomalous floquet insulators in strongly coupled nanophotonic lattices, *Phys. Rev. Lett.* **124**, 253601 (2020).
26. H. Sambe, Steady states and quasi-energies of a quantum mechanical system in an oscillating field, *Phys. Rev. A* **7**, 2203 (1973).
27. A. A. Pervishko, D. Yudin, and I. A. Shelykh, Impact of high-frequency pumping on anomalous finite-size effects in three-dimensional topological insulators, *Phys. Rev. B* **97**, 075420 (2018).
28. R. Chen, B. Zhou, and D.-H. Xu, Floquet Weyl semimetals in light-irradiated type-II and hybrid line node semimetals, *Phys. Rev. B* **97**, 155152 (2018); R. Chen, D.-H. Xu, and B. Zhou, Floquet topological insulator phase in a Weyl semimetal thin film with disorder, *Phys. Rev. B* **98**, 235159 (2018).
29. N. Goldman and J. Dalibard, Periodically Driven Quantum Systems: Effective Hamiltonians and Engineered Gauge Fields, *Phys. Rev. X* **4**, 031027 (2014); A. Eckardt and E. Anisimovas, High-frequency approximation for periodically driven quantum systems from a Floquet-space perspective, *New J. Phys.* **17**, 093039 (2015).
30. Y. Yang, Z. Xu, L. Sheng, B. Wang, D. Y. Xing, and D. N. Sheng, Time-reversal-symmetry-broken quantum spin Hall effect, *Phys. Rev. Lett.* **107**, 066602(2011).
31. Y. Zhang, C.-X. Liu, X.-L. Qi, X. Dai, Z. Fang, and S.-C. Zhang, Topological insulators in  $\text{Bi}_2\text{Se}_3$ ,  $\text{Bi}_2\text{Te}_3$  and  $\text{Sb}_2\text{Te}_3$  with a single Dirac cone on the surface, *Nat. Phys.* **5** 438 (2009).
32. X.-L. Qi, Y.-S. Wu, and S.-C. Zhang, Topological quantization of the spin hall effect in two-dimensional paramagnetic semiconductors, *Phys. Rev. B* **74**, 085308 (2006).
33. X.-L. Qi and S.-C. Zhang, Topological insulators and superconductors, *Reviews of Modern Physics* **83**, 1057 (2011).
34. B. A. Bernevig, T. L. Hughes, and S.-C. Zhang: *Science* **314**, 1757 (2006).
35. There should be a surface Dirac cone or at least a Kramers degeneracy at  $k=0$ . See for comparison the Dirac cone topological surface states at TRIMS calculated by DFT [F. Lu](#), [J. Zhou Zhao](#), [H. Weng](#), [Z. Fang](#), [Xi Dai](#) *Phys. Rev. Lett.* **110**, 096401 (2013).

---

36. W. Ruan, C. Ye, M. Guo, F. Chen, X. Chen, G.-Ming Zhang, and Y. Wang, *Phys. Rev. Lett.* **112**, 136401 (2014).
37. S. Röbner, T.-Hwan Jang, D.-Jeong Kim, and S. Wirth, *Proc. Natl. Acad. Sci. U.S.A.*, **111** (13) 4798 (2014). <https://doi.org/10.1073/pnas.1402643111>.
38. Neupane, M., Alidoust, N., Xu, S.Y. *et al.* Surface electronic structure of the topological Kondo-insulator candidate correlated electron system  $\text{SmB}_6$ . *Nat Commun* **4**, 2991 (2013). <https://doi.org/10.1038/ncomms3991>.
39. Jiang, J., Li, S., Zhang, T. *et al.* Observation of possible topological in-gap surface states in the Kondo insulator  $\text{SmB}_6$  by photoemission. *Nat Commun* **4**, 3010 (2013). <https://doi.org/10.1038/ncomms4010>.
40. Xu, N., Biswas, P., Dil, J. *et al.* Direct observation of the spin texture in  $\text{SmB}_6$  as evidence of the topological Kondo insulator. *Nat Commun* **5**, 4566 (2014). <https://doi.org/10.1038/ncomms5566>.
41. S. Kohler, J. Lehmann, and P. Hänggi, *Phys. Rep.* **406**, 379 (2005).



42. D. Thuberg, E. Muñoz, S. Eggert, and S. A. Reyes, *Phys. Rev. Lett.* 119, 267701 (2017).
43. G. Stefanucci, S. Kurth, A. Rubio, and E. K. U. Gross, *Phys. Rev. B* 77, 075339 (2008).
44. B. H. Wu and J. C. Cao, *J. Phys.: Condens. Matter* 20, 085224 (2008).
45. D. Rai and M. Galperin, *J. Phys. Chem. C* 117, 13730 (2013).
46. J. Lehmann, S. Kohler, P. Hnggi, and A. Nitzan, *Phys. Rev. Lett.* 88, 228305 (2002).
47. B. H. Wu and C. Timm, *Phys. Rev. B* 81, 075309 (2010).
48. B. H. Wu and J. C. Cao, *Phys. Rev. B* 73, 245412 (2006).
49. N. Tsuji, T. Oka, and H. Aoki, *Phys. Rev. B* 78, 235124 (2008).
50. B. H. Wu and J. C. Cao, *Phys. Rev. B* 81, 085327 (2010).
51. N. Xu, P.K. Biswas, J.H. Dil, R.S. Dhaka, G. Landolt, S. Muff, C.E. Matt, X. Shi, N.C. Plumb, M. Radović, E. Pomjakushina, K. Conder, A. Amato, S.V. Borisenko, R. Yu, H.-M. Weng, Z. Fang, X. Dai, J. Mesot, H. Ding, M. Shi, *Nat. Commun.* 5, 4566 (2014).
52. S. Suga et al., *J. Phys. Soc. Jpn* 83, 014705 (2014).
53. Hlawenka, P., Siemensmeyer, K., Weschke, E. *et al.* Samarium hexaboride is a trivial surface conductor. *Nat Commun* 9, 517 (2018). <https://doi.org/10.1038/s41467-018-02908-7>
54. A. Manchon, H. C. Koo, J. Nitta, S. M. Frolov, and R. A. Duine, New perspectives for rashba spin–orbit coupling, *Nat. Mater.* 871(2015).
55. I. Paul, C. P'epin, and M. Norman, *Phys. Rev. Lett.* 98, 026402 (2007).
56. V. Alexandrov, P. Coleman, O. Erten, *Phys. Rev. Lett.* 114, 177202 (2015).
57. Y. Sato et al., *Nat. Phys.* 15, 954 (2019).
58. Fuhrman, W.T., Chamorro, J.R., Alekseev, P. *et al.* Screened moments and extrinsic in-gap states in samarium hexaboride. *Nat Commun* 9, 1539 (2018). <https://doi.org/10.1038/s41467-018-04007-z>
59. In fact, we have the literature where it is reported that the material may show a linear T-term in the specific heat which has a coefficient that varies between 2 and 25 mJ/mole/K<sup>2</sup>, depending upon the sample preparation [7, 16, 17]. Doping with 5% of magnetic impurities can lead to an order of magnitude increase in the heat capacity [18].
60. M. E. Boulanger et al., *Phys. Rev. B.* 97, 245141 (2018).
61. Y. Xu et al., *Phys. Rev. Lett.* 116, 246403 (2016).
62. M. Orendáč, et al. Isosbestic points in doped SmB<sub>6</sub> as features of universality and property tuning. *Phys. Rev. B* 96, 115101 (2017).
63. S. Sen et al., *Physical Review Research* 2, 033370 (2020).
64. Chowdhury, D., Sodemann, I. & Sentil, T., *Nat. Commn.* 9, 1766 (2018).
65. G. Li et al., *Science*, 346, 1208–1212(2014). This study is the first report of the quantum oscillations in magnetization in Kondo insulators.
66. B.S.Tan, Y.T.Hsu, B.Zeng, M.C. Hatnean, N. Harrison, Z. Zhu, M. Hartstein, M. Kiourlappou, A. Srivastava, M. D. Johannes, et al. Unconventional Fermi surface in an insulating state. *Science*, 349, 287–290( 2015).
67. M. Hartstein, W.H.Toews, Y.T. Hsu, B. Zeng, X. Chen, M.C. Hatnean, Q.R. Zhang, S. Nakamura, A.S. Padgett, G.Rodway-Gant, et al.,*Nat. Phys.* 14, 166–172(2018).
68. Flachbart, K.; Gabáni, S.; Neumaier, K.; Paderno, Y.; Pávlík, V.; Schuberth, E.; Shitsevalova, N. Specific heat of SmB<sub>6</sub> at very low temperatures. *Physica. B* 378, 610–611(2006).
69. G. Baskaran, arXiv: 1507.03477 v1 (2015).
70. Knolle, J. & Cooper, N. R., *Phys. Rev. Lett.* 118, 096604 (2017).

71. Erten, O., Chang, P.-Y., Coleman, P. & Tsvetlik, A. M., *Phys. Rev. Lett.* 119, 057603 (2017).
72. Chowdhury, D., Sodemann, I. & Sentil, T., *Nat. Commn.* 9, 1766 (2018).
73. Sodemann, I., Chowdhury, D. & Sentil, T., *Phys. Rev. B* 97, 045152 (2018).
74. Shen, H. and Fu, L., *Phys. Rev. Lett.* 121, 026403 (2018).
75. Z. Xiang, Y. Kasahara, T. Asaba, B. Lawson, C. Insman, Lu Chen, K. Sugimoto, S. Kawaguchi, Y. Sato, G. Li, S. Yao, Y.L. Chen, F. Iga, J. Singleton, Y. Matsuda, and L. Li, *Science* 69, 65 (2018).
- 
76. P. G. LaBarre et al., arXiv:2204.05392v1 (2022), To be published in JPCM.
77. M. Orendáč, S. Gabáni, G. Pristáň, E. Gažo, P. Diko, P. Farkašovský, A. Levchenko, N. Shitsevalova and K. Flachbart, “Isosbestic Points in Doped SmB<sub>6</sub> as features of Universality and Property Tuning”, *Phys. Rev. B*, 96, 115101 (2017).
78. J. Stankiewicz, M. Evangelisti, P.F.S. Rosa, P. Schlottmann and Z. Fisk, “Physical Properties of SmxB<sub>6</sub> Single Crystals”, *Phys. Rev. B*, 99, 045138 (2019).
79. Fuhrman, W.T., Chamorro, J.R., Alekseev, P. *et al.* Screened moments and extrinsic in-gap states in samarium hexaboride. *Nat Commun* 9, 1539 (2018). <https://doi.org/10.1038/s41467-018-04007-z>
80. In fact, we have the literature where it is reported that the material may show a linear T-term in the specific heat which has a coefficient that varies between 2 and 25 mJ/mole/K<sup>2</sup>, depending upon the sample preparation [7, 16, 17]. Doping with 5% of magnetic impurities can lead to an order of magnitude increase in the heat capacity [18].
81. Z.Xiang et al., *Science* 362, 65-69 (2018).
82. S. Sen et al., *Physical Review Research* 2, 033370 (2020).
83. P F S Rosa and Z Fisk, *Bulk and Surface Properties of SmB<sub>6</sub> Rare-Earth Borides*, ed Inosov D S (New York: Jenny Stanford Publishing) chap 11(2021).
84. Kasuya, T., Takegahara, K., Fujita, T., Tanaka, T. and Bannai, E. Valence fluctuating state in SmB<sub>6</sub>. *J. Phys. Colloq.* 40, C5-308 (1979).
85. M. Orendáč, et al. Isosbestic points in doped SmB<sub>6</sub> as features of universality and property tuning. *Phys. Rev. B* 96, 115101 (2017).
86. W. Phelan et al., Correlation between bulk thermodynamic measurements and the low-temperature-resistance plateau in SmB<sub>6</sub>. *Phys. Rev. X* 4, 031012 (2014).
87. Riseborough, P. S. Collapse of the coherence gap in Kondo semiconductors. *Phys. Rev. B* 68, 235213 (2003).
88. Gabáni, S. et al. Magnetic properties of SmB<sub>6</sub> and Sm<sub>1-x</sub>La<sub>x</sub>B<sub>6</sub> solid solutions. *Czechoslov. J. Phys.* 52, A225-A228 (2002).
89. M. Abele, X. Yuan, and P. S. Riseborough, *Phys. Rev. B* 101, 094101 – Published 2 March 2020.
90. H. Eleuch and I. Rotter, *Phys. Rev. A* 95, 022117 (2017).
91. Bo Zhen, Chia Wei Hsu, Yuichi Igarashi, Ling Lu, Ido Kaminer, Adi Pick, Song-Liang Chua, John D. Joannopoulos and Marin Soljacic, *Nature*, 525, 354(2015).
92. M. Dzero, J. Xia, V. Galitski, and P. Coleman, *Annual Review of Condensed Matter Physics*, 7, 249 (2016).

---

### **Statement Regarding Data Analyzed**

All data used or analyzed during this study are included in this article.

## Appendix A

**Eigenvalues of the matrix in Eq.(8):** The functions appearing in Eq. (8) are given in Eq.8(a). There are terms of  $O(a^4q^4)$ ,  $O(a^4k^4)$ , and higher in the Hamiltonian (8) which have not been taken into account for the graphics, etc. above. The eigenvalues of the matrix in Eq.(8) are given by the quartic  $\epsilon_j^4 + a \epsilon_j^3 + b \epsilon_j^2 + c \epsilon_j + d = 0$  in Eq.(13). The coefficients  $(a, b, c, d)$  of the quartic are given by

$$a = -2(\epsilon_d + \epsilon_c), \epsilon_d = (\epsilon(k, q, \mu, b) + \vartheta(k, q, b)), \epsilon_c = (\epsilon(k, q, \mu, b) - \vartheta(k, q, b)), \quad (\text{A.1})$$

$$b = (AB + CD) + 4\epsilon_d\epsilon_c + \epsilon_c^2 + 2(d_1^2 + d_2^2 + d_3^2), \quad (\text{A.2})$$

$$c = -2(\epsilon_c AB + \epsilon_d CD + (\epsilon_d + \epsilon_c)(d_1^2 + d_2^2 + d_3^2)), \quad (\text{A.3})$$

$$d = [ABCD + (AD + BC)(d_1^2 + d_2^2) + (AC + BD)d_3^2 + (d_1^2 + d_2^2 + d_3^2)^2], \quad (\text{A.4})$$

$$A = (\epsilon_d + M), B = (\epsilon_d - M), C = (\epsilon_c + M), D = (\epsilon_c - M). \quad (\text{A.5})$$

The following symbols are defined in the main text:  $d_0 = \frac{\epsilon_d - \epsilon_c}{2}$ ,  $d_1 = -iA_1ak_y$ ,  $d_2 = iA_1ak_x$ ,  $d_3 = A_1a\chi$ , and the hybridization parameter  $A_1 = 2Vb$ . The functions appearing in Eq. (14) are given by

$$\eta_0(k) = \frac{2b_0(k)}{3} + (\Delta(k) - \Delta_0(k))^{\frac{1}{3}} - (\Delta(k) + \Delta_0(k))^{\frac{1}{3}}, \quad \Delta_0(k) = \left(\frac{b_0^3(k)}{27} - \frac{b_0(k)d_0(k)}{3} - c_0^2(k)\right), \quad (\text{A.6})$$

$$\Delta(k) = \left(\frac{2}{729}b_0^6 + \frac{4d_0^2b_0^2}{27} + c_0^4 - \frac{d_0b_0^4}{81} - \frac{2b_0^3}{27} + \frac{2c_0^2b_0d_0}{3} + \frac{d_0^3}{27}\right)^{1/2}, \quad b_0(k) = \left\{\frac{3a^2 - 8b}{16}\right\}, \quad (\text{A.7})$$

$$c_0(k) = \left\{\frac{-a^3 + 4ab - 8c}{32}\right\}, \quad d_0(k) = \frac{-3a^4 + 256d - 64ac + 16a^2b}{256}. \quad (\text{A.8})$$

## Appendix B

**Eigenvectors of the matrix in Eq.(8):** We present here the eigenstates linked to the eigenvalues in  $\epsilon_j$  ( $s, \sigma, k, q, \mu, b, M$ ) in (13). These will be required for the calculation of the Chern number when  $M \neq 0$ . These Bloch states are given by

$$|\psi^{(j)}(k)\rangle = \begin{pmatrix} \psi_1^j(k) \\ \psi_2^j(k) \\ \psi_3^j(k) \\ \psi_4^j(k) \end{pmatrix}, \quad j=1, 2, 3, 4, \quad (\text{B.1})$$

$$\psi_1^j(k) = g_1^j(k), \quad \psi_2^j(k) = (-iak_+)f_2^j(k)g_1^j(k), \quad \psi_3^j(k) = i(\epsilon_j - \epsilon_d + M)f_3^j(k)g_1^j(k),$$

(B.2)

$$\psi_4^j(k) = (-A_1 a k_+) f_4^j(k) g_1^j(k), \quad (\text{B.3})$$

$$g_1^j(k) = \Upsilon_j^{-1/2}(k) = (1 + a^2 k^2 |f_2^j(k)|^2 + (\epsilon_j - \epsilon_d + M)^2 |f_3^j(k)|^2 + A_1^2 a^2 k^2 |f_4^j(k)|^2)^{-\frac{1}{2}}, \quad (\text{B.4})$$

$$f_2^j(k) = (aq)^{-1} [(\epsilon_j - \epsilon_d - M)(\epsilon_j - \epsilon_c + M) + A_1^2 a^2 k^2 + A_1^2 a^2 q^2] \times [(\epsilon_j - \epsilon_d + M)(\epsilon_j - \epsilon_c + M) + A_1^2 a^2 k^2 + A_1^2 a^2 q^2]^{-1} \quad (\text{B.5})$$

$$f_3^j(k) = (A_1 a q)^{-1} [(\epsilon_j - \epsilon_d - M)(\epsilon_j - \epsilon_c + M) + A_1^2 a^2 k^2 + \eta A_1^2 a^2 q^2] \times [(\epsilon_j - \epsilon_d + M)(\epsilon_j - \epsilon_c + M) + A_1^2 a^2 k^2 + A_1^2 a^2 q^2]^{-1}, \quad \eta = \frac{(\epsilon_j - \epsilon_d - M)}{(\epsilon_j - \epsilon_d + M)}, \quad (\text{B.6})$$

$$f_4^j(k) = 2M / [(\epsilon_j - \epsilon_d + M)(\epsilon_j - \epsilon_c + M) + A_1^2 a^2 k^2 + A_1^2 a^2 q^2]. \quad (\text{B.7})$$

Here  $\epsilon_j = \epsilon_j(s, \sigma, k, b, M)$  is given by Eq. (14). In the special case  $M \rightarrow 0$ ,  $\psi_1^j(k) = \Upsilon_j^{-1/2}(k)$ ,  $\psi_2^j(k) = \frac{d_1 + i d_2}{d_3} \Upsilon_j^{-1/2}(k)$ ,  $\psi_3^j(k) = \frac{(\epsilon_j - \epsilon_d)}{d_3} \Upsilon_j^{-1/2}(k)$ , and  $\psi_4^j(k) = 0$ . We find that the function  $\Upsilon_j^{-1/2}(k)$  is given by  $\frac{aq}{\left[ \frac{(\epsilon_j - \epsilon_d)^2}{A_1^2} + (ak)^2 + (aq)^2 \right]^{1/2}}$ . The eigenvectors in this special case are

$$|\psi^{(j)}(k)\rangle = \begin{pmatrix} \frac{aq}{\left[ \frac{(\epsilon_j - \epsilon_d)^2}{A_1^2} + (ak)^2 + (aq)^2 \right]^{1/2}} \\ -iak_+ \\ \frac{(\epsilon_j - \epsilon_d)}{A_1} \\ \frac{aq}{\left[ \frac{(\epsilon_j - \epsilon_d)^2}{A_1^2} + (ak)^2 + (aq)^2 \right]^{1/2}} \\ 0 \end{pmatrix}. \quad (\text{B.8})$$

## Appendix C

**Z<sub>2</sub> invariant of the system:** We wish to calculate the Z<sub>2</sub> invariant of the system in order to show that SmB<sub>6</sub> is indeed a strong TI. We feel necessary to outline the method [12] in an effort to make the present communication comprehensive. We consider the green and red bands in Figure 2(a) and (b), and denote their Bloch wave functions, respectively, as  $|\psi^{(1)}(k)\rangle$  and  $|\psi^{(2)}(k)\rangle$  for this purpose, where following Fu and Kane[12] we assume the system one dimensional, i.e.  $\mathbf{k} = (k, 0)$ . We impart the time dependence assuming that the band parameters change with time and

return to the original values at  $t = T$ . We also suppose that the Hamiltonian  $h_{\text{surface}}^{\text{BHZ}} (M = 0)$  satisfies the following conditions  $h_{\text{surface}}^{\text{BHZ}} (M = 0, -t) = \Theta h_{\text{surface}}^{\text{BHZ}} (M = 0, t) \Theta^{-1}$  and  $h_{\text{surface}}^{\text{BHZ}} (M = 0, t + T) = h_{\text{surface}}^{\text{BHZ}} (M = 0, t)$ . It is well-known [12] that charge polarization  $P$  can be calculated by integrating the Berry connection of the occupied states over the BZ. In the present case of the two-band system,  $P$  may be written as  $P = P_1 + P_2$  where the Berry connections  $\{-i\langle \dot{u}^{(\alpha)}(k) | \nabla_k | \dot{u}^{(\alpha)}(k) \rangle\}$  are given by  $c_{\alpha\alpha}(k)$  ( $\alpha = 1, 2$ ) and

$$P_1 = \int_{-\pi}^{\pi} \frac{dk}{2\pi} c_{11}(k), \quad P_2 = \int_{-\pi}^{\pi} \frac{dk}{2\pi} c_{22}(k). \quad (\text{C.1})$$

The Berry curvature is given by  $\Omega_{\alpha}(k) = \nabla_k \times c_{\alpha\alpha}(k)$ . The total polarization density  $C(k) = c_{11}(k) + c_{22}(k)$ . This yields the TR polarization which is defined by  $P_{tr} = P_1 - P_2 = 2P_1 - P$ . Here  $P_{tr}$  gives the difference in charge polarization between spin-up and spin-down quasiparticle bands. We now go back the charge polarization  $P$ , calculated by integrating the Berry connection of the occupied states over the BZ. Furthermore, the time-reversed version of  $|\dot{u}^{(2)}(k)\rangle$  is equal to  $|\dot{u}^{(1)}(-k)\rangle$  except for a phase factor. Hence, at  $t = 0$  and  $t = T/2$  one may write  $\Theta|\dot{u}^{(2)}(k)\rangle = e^{-i\rho(k)}|\dot{u}^{(1)}(-k)\rangle$  and  $\Theta|\dot{u}^{(1)}(k)\rangle = -e^{-i\rho(-k)}|\dot{u}^{(2)}(-k)\rangle$ . It is not difficult to see that the matrix representation of the TR operator  $\Theta$  in the Bloch wave function basis  $\xi_{\alpha\beta}(k) \equiv \langle \dot{u}^{(\alpha)}(-k) | \Theta | \dot{u}^{(\beta)}(k) \rangle$  will now be given as  $\xi(k) = \begin{pmatrix} 0 & e^{-i\rho(k)} \\ -e^{-i\rho(k)} & 0 \end{pmatrix}$ . One can easily confirm that  $\xi_{\alpha\beta}(k)$  is a unitary matrix. It has the property  $\xi_{\alpha\beta}(-k) = -\xi_{\alpha\beta}(k)$ . This implies that  $\xi_{\alpha\beta}(k)$  is anti-symmetric at a TRIM. Upon getting back to the connections, we note that the connections satisfy  $c_{11}(-k) = c_{22}(k) - \frac{\partial}{\partial k} \rho(k)$ . These lead us to the charge polarization between spin-up bands  $P_1$  as  $P_1 = \int_0^{\pi} \frac{dk}{2\pi} C(k) - \frac{i}{2\pi} [\rho(\pi) - \rho(0)]$ . Since  $\rho(k) = i \log \xi_{12}(k)$ , and  $C(k) = \text{tr}(c(k))$ , after a little algebra, we find

$$P_{tr} = \frac{1}{i\pi} \log \left( \frac{\sqrt{\xi_{12}(0)^2}}{\xi_{12}(0)} \cdot \frac{\xi_{12}(\pi)}{\sqrt{\xi_{12}(\pi)^2}} \right). \quad (\text{C.2})$$

Obviously enough, the argument of the logarithm is  $+1$  or  $-1$ . Furthermore, since  $\log(-1) = i\pi$  one can see that  $P_{tr}$  is 0 or 1 (mod 2). Physically, of course, the two values of  $P_{tr}$  corresponds to two different polarization states which the system can take at  $t = 0$  and  $t = T/2$ . The Bloch functions  $|\dot{u}^{(\alpha)}(k, t)\rangle$  introduced above could be visualized as maps from the 2D phase space  $(k, t)$  to the Hilbert space. As in refs. [12], the Hilbert space could be separated into two parts depending on the difference in  $P_{tr}$  between  $t = 0$  and  $t = T/2$ . This leads to introduction of a quantity  $\nu_0$ , specified only in mod 2, and defined as  $(P_{tr}(\frac{T}{2}) - P_{tr}(0))$ : When  $P_{tr}$  does not changes between  $t = 0$  to  $T/2$ ,  $\nu_0 = 0$ , whereas if there is a change then  $\nu_0 = 1$ . The visualization mentioned above, thus, yields that the Hilbert space is trivial if  $\nu_0 = 0$ , while for  $\nu_0 = 1$  it is nontrivial (twisted). Equivalently, the system band structures are characterized by Kane–Mele index [12, 73]  $Z_2 = +1$  ( $\nu_0 = 0$ ) and  $Z_2 = -1$  ( $\nu_0 = 1$ ). We obtain

$$(-1)^{\nu_0} = \prod_j \frac{\xi_{12}(\mathbf{k}_{\text{trim}}^{(j)})}{\sqrt{\xi_{12}(\mathbf{k}_{\text{trim}}^{(j)})^2}}. \quad (\text{C.3})$$

We now consider the generalization of this result. For this purpose, we suppose that  $2N$  bands are occupied and forming  $N$  Kramers pairs. For each such pair  $n$ , at the TR symmetric times  $t = 0$  and  $\pi$  the wave functions are related by write  $\Theta|\dot{u}_n^{(2)}(\mathbf{k})\rangle = e^{-i\rho_n(k)}|\dot{u}_n^{(1)}(-\mathbf{k})\rangle$  and  $\Theta|\dot{u}_n^{(1)}(\mathbf{k})\rangle = e^{-i\rho_n(k)}|\dot{u}_n^{(2)}(-\mathbf{k})\rangle$  and the matrix  $\xi(k) =$

$$\begin{pmatrix} 0 & e^{-i\rho_1(k)} & 0 & 0 & \dots \\ -e^{-i\rho_1(-k)} & 0 & 0 & 0 & \dots \\ 0 & 0 & 0 & e^{-i\rho_2(k)} & \dots \\ 0 & 0 & -e^{-i\rho_2(-k)} & 0 & \dots \\ \vdots & \vdots & \vdots & \vdots & \ddots \end{pmatrix}. \quad (\text{C.4})$$

This leads to  $\xi_{12}(\mathbf{k}_{\text{trim}}^{(j)})\xi_{34}(\mathbf{k}_{\text{trim}}^{(j)})\dots\dots\dots\xi_{2N-1,2N}(\mathbf{k}_{\text{trim}}^{(j)}) = e^{-i\sum_{n=1}^N\rho_n(\mathbf{k}_{\text{trim}}^{(j)})} = \text{Pf}[\xi(\mathbf{k}_{\text{trim}}^{(j)})]$ , where Pfaffian is defined for an antisymmetric matrix and is related to the determinant by  $\text{Pf}[A]^2 = \det[A]$ . The difference in charge polarization between spin-up and spin-down quasiparticle bands, in this general case, is now given by  $P_{tr} = \frac{1}{i\pi} \log\left(\frac{\sqrt{\det[\xi(0)]}}{\text{Pf}[\xi(0)]} \cdot \frac{\text{Pf}[\xi(\pi)]}{\sqrt{\det[\xi(0)]}}\right)$ . Thus, the  $Z_2$  topological invariant  $\nu$  is given by  $(-1)^{\nu_0} = \prod_j \delta(\mathbf{k}_{\text{trim}}^{(j)})$  where for each TRIM  $\mathbf{k}_{\text{trim}}^{(j)}$  one defines

$$\delta(\mathbf{k}_{\text{trim}}^{(j)}) \equiv \frac{\text{Pf}[\xi(\mathbf{k}_{\text{trim}}^{(j)})]}{\sqrt{\det[\xi(\mathbf{k}_{\text{trim}}^{(j)})]}}. \quad (\text{C.5})$$

As we see in the section 3 of the main text, this leads to the classification of the Hilbert space into the twisted ( $\nu_0 = 1$ ) and the trivial one ( $\nu_0 = 0$ ).

## Appendix D

**Chern number calculation:** We calculate here the intrinsic anomalous Hall conductivity (AHC)/Chern number to show that the system is in the quantum anomalous Hall (QAH) phase when  $M \neq 0$ . The expression of AHC is

$$\sigma_{AH} = -\left(\frac{e^2}{h}\right) \sum_j \int_{BZ} \frac{d^2k}{(2\pi)^3} g(E_j(k) - \mu) \Omega_j^z(k), \quad (\text{D.1})$$

where  $\mu$  is the chemical potential of the fermion number,  $j$  is the occupied band index,  $g(E_j(k) - \mu)$  is the Fermi-Dirac distribution and  $\Omega_j^z(k)$  is the  $z$ -component of the Berry curvature (BC) for the  $j$ th band. To obtain AHC, we calculate BC using the Kubo formula

$$\Omega_j^z(k) = -2\hbar^2 \text{Im} \sum_{i \neq j} (E_j(k) - E_i(k))^{-2} \langle j, k | \widehat{v}_x | i, k \rangle \langle i, k | \widehat{v}_y | j, k \rangle. \quad (\text{D.2})$$

Here  $\mathbf{k}$  is the Bloch wave vector,  $E_j(\mathbf{k})$  is the band energy,  $|j, \mathbf{k}\rangle$  are the Bloch functions of a single band. The operator  $\hat{v}_j$  represents the velocity in the  $j$  direction. For a system in a periodic potential and its Bloch states as the eigenstates, in view of the Heisenberg equation of motion  $i\hbar \frac{d\hat{x}}{dt} = [\hat{x}, \hat{H}]$ , the identity  $\langle m, \mathbf{k}' | \hat{v}_\alpha | n, \mathbf{k} \rangle = \left(\frac{1}{\hbar}\right) (E_j(\mathbf{k}') - E_i(\mathbf{k})) \langle i, \mathbf{k}' | \frac{\partial}{\partial k_\alpha} | j, \mathbf{k} \rangle$  is satisfied. Upon using this identity, we obtain AHC in the zero temperature limit as  $\sigma_{\text{AH}} = C \left(\frac{e^2}{\hbar}\right)$  where  $C = \sum_j C_j$ ,  $C_j = \int \int_{\text{BZ}} \Omega_{\text{xy}}(k) \frac{d^2k}{(2\pi)^2}$ . The z-component of the Berry-curvature(BC) is

$$\Omega_{\text{xy}}(k) = \sum_j \left( \frac{\partial A_{j,y}}{\partial k_x} - \frac{\partial A_{j,x}}{\partial k_y} \right) = -2 \sum_j \text{Im} \left\langle \frac{\partial \psi_{j,\mathbf{k}}}{\partial k_x} \left| \frac{\partial \psi_{j,\mathbf{k}}}{\partial k_y} \right. \right\rangle \quad (\text{D.3})$$

where  $\psi_{j,\mathbf{k}} = |j, \mathbf{k}\rangle$ . The vector potential  $A_j(\mathbf{k})$  is the Berry connection and  $\nabla_{\mathbf{k}} \times A_j(\mathbf{k}) = \Omega_j(\mathbf{k})$  is the Berry curvature (BC). We use the results presented in appendices A and B, and Eq. (D.3) to calculate BC. Next, upon integrating BC on a  $k$ -mesh-grid of the Brillouin zone, we calculate the intrinsic AHC.